Super Resolution Technique for GPR Detection of Layered Media

Amit Sarkar
Roll No. 213EC6269

Department of Electronics and Communication Engineering
National Institute of Technology, Rourkela
Rourkela, Odisha, India
2015

Super Resolution Technique for GPR Detection of Layered Media

Thesis submitted in partial fulfillment of the requirements for the degree of

Master of Technology

in

Signal & Image Processing

by

Amit Sarkar

Roll No. 213EC6256

under the guidance of

Prof. Subrata Maiti

Department of Electronics and Communication Engineering

National Institute of Technology, Rourkela

Rourkela, Odisha, India

2015

Dedicated to my family...

National Institute of Technology
Rourkela

CERTIFICATE

This is to certify that the work in the thesis entitled **Super Resolution Technique for GPR Detection of Layered Media"** submitted by ***Amit Sarkar*** is a record of an original research work carried out by him under my supervision and guidance in partial fulfillment of the requirements for the award of the degree of **Master of Technology** in **Signal & Image Processing** from National Institute of Technology, Rourkela. Neither this thesis nor any part of it, to the best of my knowledge, has been submitted for any degree or academic award elsewhere.

Prof. Subrata Maiti
Assistant Professor
Department of ECE
National Institute of Technology
Rourkela

National Institute of Technology
Rourkela

DECLARATION

I certify that

1. The work contained in the thesis is original and has been done by myself under the supervision of my supervisor.
2. The work has not been submitted to any other Institute for any degree or diploma.
3. Whenever I have used materials (data, theoretical analysis, and text) from other sources, I have given due credit to them by citing them in the text of the thesis and giving their details in the references.
4. Whenever I have quoted written materials from other sources, I have put them under quotation marks and given due credit to the sources by citing them and giving required details in the references.

Amit Sarkar

Acknowledgment

This work is one of the most important achievements of my career. Completion of my project would not have been possible without the help of many people, who have constantly helped me with their full support for which I am highly thankful to them.

First of all, I would like to express my gratitude to my supervisor **Prof. Subrata Maiti**, who has been the guiding force behind this work. I want to thank him for giving me the opportunity to work under him. He is not only a good Professor with deep vision but also a very kind person. I consider it my good fortune to have got an opportunity to work with such a wonderful person.

I am obliged to **Prof. K.K. Mahapatra**, HOD, Department of Electronics and Communication Engineering for creating an environment of study and research. I am also thankful to Prof. A.K Swain, Prof. L.P. Roy, Prof. S. Meher, Prof. A.K. Sahoo, Prof. D.P. Acharya and Prof. S. Ari for helping me how to learn. They have been great sources of inspiration.I would like to thank all faculty members and staff of the ECE Department for their sympathetic cooperation.

When I look back at my accomplishments in life, I can see a clear trace of my family's concerns and devotion everywhere. My dearest mother, whom I owe everything I have achieved and whatever I have become; my beloved father, who always believed in me and inspired me to dream big even at the toughest moments of my life; and my brother; who were always my silent support during all the hardships of this endeavor and beyond.

I have been blessed with friends who have always supported and guided me. And a special appreciation goes to a close friend who have always motivated me to do the right thing in the right manner.

Amit Sarkar

Abstract

Ground Penetrating Radar is one of the most popular non-destructive subsurface exploration system available to us. Due to the advent of technology in the field of remote sensing, GPR systems have been put to use in a wide variety of applications. Here we are concerned with the extraction of layered media properties. Exploration of layered medias have become an important part in the progress of road development. In order to obtain the necessary layered media parameters, different signal processing methods have been put to use. As the received GPR signal is obtained in spectral domain, different Super-Resolution algorithms were put to use. Their need is felt when we come across very thin layered media. By using normal IFFT inversion technique, we are unable to resolve very closely spaced targets, which are below its range resolution. These spectral estimation techniques paves the way for layer stripping approach to obtain the necessary layered media parameters. Layer stripping is an effective, timing efficient method used for practical field applications. We also have inversion approach of full wave modelling. It gives us accurate estimates of underground layered media properties. But the main drawback is its complexity and time consuming nature. This feature makes it very difficult to provide instantaneous results during field operations.

As a result, depending upon the nature of application involved, we can implement either layer stripping or full wave modelling approach. But in general, if pin point accuracy is not needed, then layer stripping approach is the better alternative.

Keywords: Ground Penetrating Radar, Super-Resolution, Layer Stripping, Full wave modelling.

Contents

Certificate **iv**

Declaration **v**

Acknowledgment **vi**

Abstract **vii**

List of Figures **xi**

List of Tables **xiii**

1 Fundamentals of GPR **1**

1.1 Introduction 1

1.2 GPR Overview 2

1.2.1 GPR Technology 2

1.2.2 Historical review 3

1.2.3 Need for GPR 4

1.2.4 Types of GPR 5

1.2.5 GPR System 6

1.3 Electro-Magnetic Properties of media 7

1.3.1 Maxwell's Equations 7

1.3.2 The Electrical Conductivity 8

1.3.3 The Dielectric Permittivity 8

1.3.4 Propagation of Electromagnetic Waves in dielectric materials . . . 8
1.3.5 Wavelet Concept . . . 10
1.4 SFCW GPR System Parameters . . . 10
1.5 Different Types of GPR Scanning Mechanism . . . 14
1.6 Signal Processing in GPR . . . 16
1.7 Problem Areas . . . 17
1.8 Problem Definition . . . 17
1.9 Thesis Overview . . . 17
1.10 Summary . . . 18

2 Subspace Spectral Estimation Techniques 19
2.1 Introduction . . . 19
2.2 Sinusoidal Model . . . 20
2.3 Signal Model for Backscattered GPR Reflections: . . . 21
2.4 Subspace Estimation Techniques . . . 23
2.4.1 Spectral MUltiple SIgnal Classification (MUSIC) : . . . 23
2.4.2 Root MUltiple SIgnal Classification (R-MUSIC): . . . 24
2.4.3 Estimation of Signal Parameters via Rotational Invariance Technique (ESPRIT): . . . 26
2.5 Signal Number Estimation . . . 30
2.6 Various Smoothing Techniques . . . 31
2.7 Summary . . . 33

3 GPR Signal Modelling for Layered Media 34
3.1 Introduction . . . 34
3.2 Plane Wave Model . . . 35
3.3 Full Wave Model . . . 37
3.3.1 VNA-Antenna-ground subsurface modelling . . . 37
3.3.2 Modelling air-subsurface with Greens function . . . 38
3.3.3 Model Inversion . . . 39

3.4 Layer Stripping Approach 40
3.4.1 Introduction 40
3.4.2 Reflection method used for Layer Stripping 40
3.4.3 Estimation of Static Dielectric Constant from Reflection Amplitudes 41
3.4.4 Estimation of Static Conductivity from Reflection Amplitudes 43
3.5 Summary 44

4 Results and Discussion **45**
4.1 Experimental Model with a Single Layered Sand 45
4.2 Results 47
4.3 Discussion 58

5 Conclusions and Future Work **59**
5.1 Conclusion 59
5.2 Future Work 60

Bibliography **61**

List of Figures

1.1 Working of a GPR 2
1.2 Types of GPR 5
1.3 General GPR System 6
1.4 General SFCW System 11
1.5 Stepped Frequency Analysis 12
1.6 Types of GPR Scans 15

2.1 Backscattering of GPR signal in layered media 21
2.2 Flowchart depicting the working of Spectral MUSIC algorithm . . 24
2.3 Flowchart depicting the working of Root MUSIC algorithm 26
2.4 Flowchart depicting the working of LS and TLS ESPRIT algorithm 29
2.5 Forward and Forward-backward Spatial Smoothing Approach . . 32

3.1 Three layered target medium 35
3.2 Block diagram representing the VNAantennamultilayered medium system 37
3.3 Model configuration of N-layered medium with a point source . . 38

4.1 SFCW- Monostatic GPR Laboratory Experimental Setup 45
4.2 Best case Effective Bandwidth using EIF order estimator with modelled data 48
4.3 Best case Effective Bandwidth using MDL order estimator with modelled data 49

4.4 Best case Effective Bandwidth using EIF order estimator with measured data 50
4.5 Best case Effective Bandwidth using MDL order estimator with measured data 51
4.6 BPCE for EIF order estimator 53
4.7 BPCE for MDL order estimator 54
4.8 Best Case parameters estimation for different TBPs from modelled data 55
4.9 Best Case parameters estimation for different TBPs from measured data 56

List of Tables

4.1 Comparison of Layered Media Parameters for Measured Data . . 57
4.2 Comparison of Layered Media Parameters for Synthetic Data . . . 57

Chapter 1

Fundamentals of GPR

1.1 Introduction

Today geophysical prospection is a standard strategy for recognizing covered archeological elements and structures. The archeological administrations depend upon these procedures at whatever point essential. The fundamental conditions require quick and precise studying of substantial regions under distinctive circumstances. Geoelectrical and geomagnetic techniques were set up in the 1960s. Considering the first instruments, the essential gadgets were not very costly and took into account boundless application and acknowledgement of these techniques. Particularly the rapid with which Earth's attractive field can be measured made an incredible commitment. The profiles and shape maps toward the starting were hard to see, notwithstanding for a pro. Speaking to these information by utilizing strategies from computerized picture handling in greyscale or shading upgraded the meaningfulness of the outcomes altogether. This made the information available for archeologists and demonstrated fine points of interest never seen. Such systems, including electromagnetics, are extremely restricted in flat and vertical determination, which one tries to overcome by reversal or tomography. Ground-Penetrating Radar (GPR) is a strategy that has the capacity to give high determination, three dimensional data. This point of interest was perceived quite a while back and now GPR has turn into a standard technique as well. The measure of information got in an overview is large to the point that exceptional treatment is

important, particularly concerning the physical phenomena included. There must be a decent geophysical foundation for understanding and right operation of such a framework, including the information preparing. This has kept archeologists from beginning to work with this strategy. The advances in ground-infiltrating radar in the previous decades have been exceptional. The greater part of the systems utilized today are normal and acknowledged strategies now.

1.2 GPR Overview

1.2.1 GPR Technology

Ground Penetrating Radar (GPR) as the name suggests, is a high-resolution electromagnetic technique applied for evaluating the spatial dimension of buried objects and to investigate the presence and continuity of natural subsurface conditions and features, without drilling, probing, or digging [1].

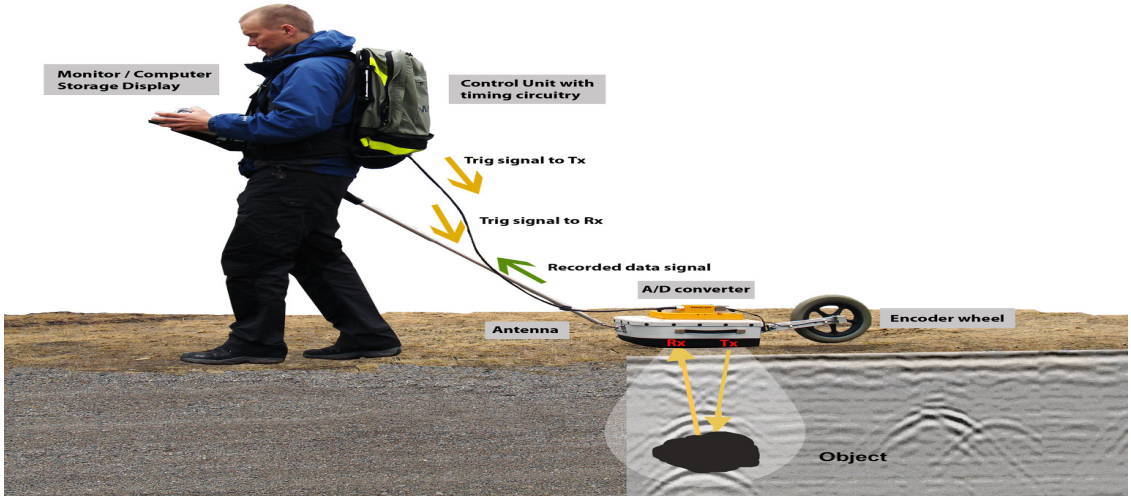

Figure 1.1: Working of a GPR

The above figure displays the working of GPR for mapping underground structures [21]. GPR operates by transmitting EM wave radiated by the transmitter into the ground. The EM wave is reflected from various underground objects or from contrasting dielectric properties , such as at the boundary between soil and a landmine or between soil and a large rock.The reflections are created by an abrupt

change with the dielectric properties in the ground. These electrical properties include, relative permittivity, relative permeability and conductivity.

Conductivity affects the maximum range of the GPR due to absorption of the EM waves in the medium. Soil with high moisture content increases conductivity, thus decreasing penetration.

Relative permeability hardly provides any valuable information because it offers little contrast in the radiated EM pulses.

Relative permittivity provides the highest degree of contrast in the reflected wave, thus resulting in good characterization of the ground. Therefore, the contrast in permittivity usually leads to the reflection in the EM pulse.

1.2.2 Historical review

The basic standards of GPR were known subsequent to the start of the twentieth century, yet the electronic parts accessible around then were not sufficiently quick to test a follow with a determination in the picosecond range. This popularity could just be satisfied in the 1960s when the first frameworks were constructed. Until today the follow is never examined all in all, yet a few heartbeats are utilized and the adequacy measured at a marginally moved time. By utilizing this trap the complete follow is reproduced. The presentation around then was an oscilloscope, where a solitary follow could be seen [2]. Recording was just conceivable by taking a photo of the screen. Later on the follows were imprinted on a paper strip in the field. Presently a record of the information was conceivable, however it was still hard to utilize these profiles on account of the entangled imaging geometry and on the grounds that it was hard to follow reflections from one profile to the next. Just with the appearance of completely advanced frameworks did GPR begin to be effective. This is the vital essential to have the capacity to process the information and to create flat arranges, like those from geoelectrical or geomagnetic routines. This began the blast in the technique in the 1980s, which endures until today.

1.2.3 Need for GPR

GPR has turn into an inexorably well known choice for archeological exploration for various reasons. These can be contracted down to four key advantages: Its non-dangerous nature; Its capacity to boost research effectiveness and minimize expense; Its capacity to cover extensive regions rapidly; and its fantastic three-dimensional information.

As it is a remote detecting system, GPR is totally non-intrusive and nondestructive, rather than ”conventional” archeological uncovering strategies, which are naturally damaging.

GPR additionally can possibly expand research proficiency. In correlation to ”conventional” archeological removal routines, GPR reviews are led rapidly and at a moderately minimal effort. At the point when utilized as a prospection strategy, GPR can help in recognizing ranges of high potential for future exhuming (or then again, recognize territories of low potential which ought to be maintained a strategic distance from), in this way amplifying significant information accumulation while minimizing time and expense, notwithstanding site sway.

At long last, GPR creates high-determination three-dimensional information suitable for tending to anthropological inquiries. The determination capacity of GPR is ”by a wide margin more noteworthy than that got by other geophysical routines.” This high-determination three dimensional information can be effortlessly coordinated with information gathered by other geophysical strategies, archeological uncovering, and surface study maps in geographic data frameworks.

1.2.4 Types of GPR

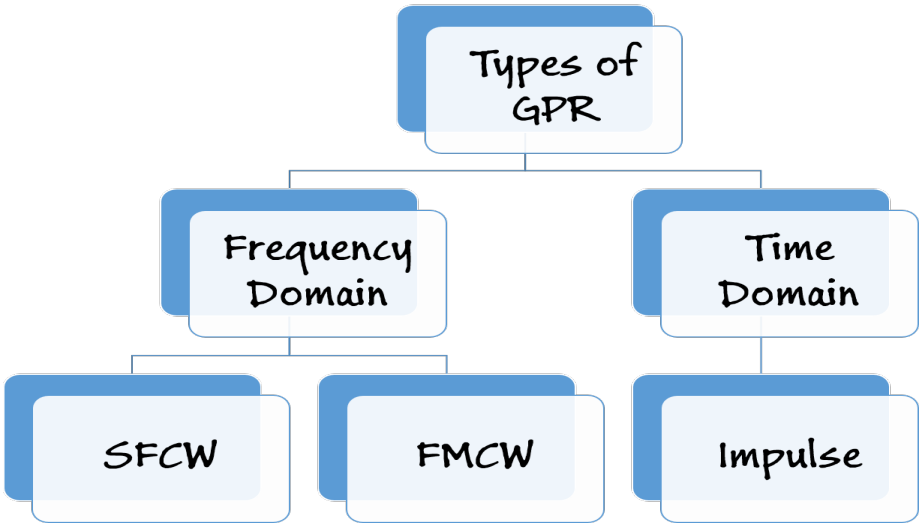

Figure 1.2: Types of GPR

1. **Time Domain**

   (a) **Impulse**: Here pulse of very short duration and hence high bandwidth is used for target detection.Range is found out by determining the time delay from the target.

   Advantages: Simple low cost circuit.
   Disadvantages: High ringing, low duty cycle.

2. **Frequency Domain**

   (a) **Frequency Modulated Continuous Waveform** (FMCW): Here the frequency from the synthesizer is varied continuously from one point to another. The range information is found out by the beat frequency.

   Advantages: Simple design and low cost for implementation.
   Disadvantages: Uncertainity in frequency sweep results in low performance.

   (b) **Stepped Frequency Continuous Waveform** (SFCW): Here the frequency is varied in equal steps and continuous signal of each frequency is sent

and received. Range information is found from the phase change between the two successive continuous signals.

Advantages: Transmit frequency in controlled way, High range, Low SNR.

Disadvantages: Complex electronics, Time consuming.

1.2.5 GPR System

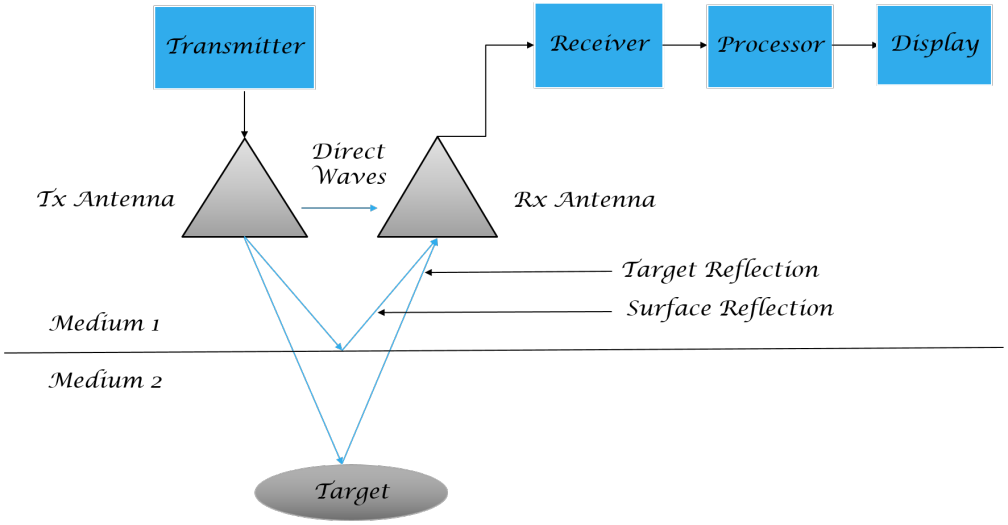

Figure 1.3: General GPR System

- Transmitter: Here the RF GPR signal is generated depending on the type of GPR system.
- The generated EM wave is transported to antenna using co-axial cables.
- After striking the target medium the reflected GPR signal is accumulated by the receiver antenna into the receiver block.
- The received signal is filtered, processed and made suitable for proper viewing of the tar-get medium.

1.3 Electro-Magnetic Properties of media

In order to understand the main ideas and principles of electromagnetic wave theory in inhomogeneous or piecewise homogeneous media, a short introduction on the fundamental equations as well as on the electromagnetic wave propagation, attenuation and reflection processes will be given.

1.3.1 Maxwell's Equations

The four equations are as follows [3]:

$$\nabla \cdot \mathbf{E} = \frac{\rho}{\varepsilon_0} \tag{1.1}$$

$$\nabla \cdot \mathbf{B} = 0 \tag{1.2}$$

$$\nabla \times \mathbf{E} = -\frac{\partial \mathbf{B}}{\partial t} \tag{1.3}$$

$$\nabla \times \mathbf{B} = \mu_0 \mathbf{J} + \mu_0 \varepsilon_0 \frac{\partial \mathbf{E}}{\partial t} \tag{1.4}$$

where $\mathbf{E}$ and $\mathbf{B}$ are the electric and magnetic field vectors, respectively, ρ is the volume charge density, $\mathbf{J}$ is the current density vector, and ε_0 and μ_0 are the dielectric permittivity and magnetic permeability of free space, respectively.

GPR involves EM waves through materials subjected to charge separation during the passage of electric field and low magnetization in a magnetic field, it makes more sense to use the following versions of Maxwell's equations:

$$\nabla \cdot \mathbf{D} = \rho_f \tag{1.5}$$

$$\nabla \cdot \mathbf{B} = 0 \tag{1.6}$$

$$\nabla \times \mathbf{E} = -\frac{\partial \mathbf{B}}{\partial t} \tag{1.7}$$

$$\nabla \times \mathbf{H} = \mathbf{J}_c + \frac{\partial \mathbf{D}}{\partial t} \tag{1.8}$$

where $\mathbf{D}$ and $\mathbf{H}$ are the electric displacement and magnetic auxiliary fields,

respectively, ρ_f is the volume free charge density, and $\mathbf{J}_c$ is the conduction or free current density.

1.3.2 The Electrical Conductivity

The electric conductivity [4] describes currents from free charge movement responding to incident electric field E. For low frequency alternative electric fields,current varies in phase with E. With higher frequency the response time increases and gives out of phase current. Therefore, the electric conductivity σ can be represented by the complex quantity

$$\sigma = \sigma' + j\sigma'' \tag{1.9}$$

1.3.3 The Dielectric Permittivity

The dielectric permittivity explain currents which result from bound charge displacement and describes material polarizability. With increasing frequency the bound charges become so slow that it cannot follow the fast alternating electric field and a relaxation phenomenon appears resulting in a out of phase polarization component. Hence the dielectric permittivity is also described by a complex quantity

$$\varepsilon = \varepsilon' - j\varepsilon'' \tag{1.10}$$

1.3.4 Propagation of Electromagnetic Waves in dielectric materials

Electromagnetic wave propagation can be shown by a one-dimensional wave equation as follows:

$$\frac{\partial^2 \mathbf{E}}{\partial z^2} = \mu\varepsilon \frac{\partial^2 \mathbf{E}}{\partial t^2} \tag{1.11}$$

A wave propagating in the positive z-direction in a perfect dielectric can be described by the following:

$$\mathbf{E}(z) = \mathbf{E}_0 e^{ikz} \tag{1.12}$$

where the phase constant is described as:

$$k = \frac{\omega}{v} = \omega\sqrt{\mu\varepsilon} \tag{1.13}$$

In a conducting dielectric the phase constant is complex and is

$$k = \omega\sqrt{\mu\left(\varepsilon' - j\varepsilon''\right)} \tag{1.14}$$

The wave number into real and imaginary parts can be described as:

$$jk = \alpha + j\beta = j\omega\sqrt{\mu\varepsilon'\left(1 - j\frac{\varepsilon''}{\varepsilon'}\right)} \tag{1.15}$$

where α is the attenuation factor and β is the phase constant.

The parameters α and β can be related to σ and $j\omega\varepsilon$, giving expressions for α and β as shown below:

$$\alpha = \omega\sqrt{\frac{\mu\varepsilon}{2}}\left[\sqrt{1 + \left(\frac{\sigma}{\omega\varepsilon}\right)^2} - 1\right]^{1/2} \tag{1.16}$$

$$\beta = \omega\sqrt{\frac{\mu\varepsilon}{2}}\left[\sqrt{1 + \left(\frac{\sigma}{\omega\varepsilon}\right)^2} + 1\right]^{1/2} \tag{1.17}$$

Here, $\tan\delta = \left(\frac{\sigma}{\omega\varepsilon}\right)^2$ is known as the loss tangent.

The velocity of propagation is also slowed by an increase of loss tangent as well as relative dielectric constant,

$$v = c\sqrt{\left[\frac{\varepsilon'}{2\varepsilon_0}\left(\sqrt{(1 + \tan^2\delta)} + 1\right)\right]} \tag{1.18}$$

But for $\tan\delta < 1$,

$$v = \frac{c}{\sqrt{\varepsilon_r}} \tag{1.19}$$

The intrinsic impedance of a medium is the relationship between the electric field, E, and the magnetic field, H and is a complex quantity which is calculated

according to:

$$\eta = \sqrt{\frac{-j\omega\mu}{\sigma - j\omega\varepsilon}} \tag{1.20}$$

When applying electromagnetic waves to measure material properties, one could basically use two different techniques:

1. Reflection
2. Transmission.

The reflected field strength is described by the reflection coefficient, R:

$$R_{12} = \frac{\eta_2 - \eta_1}{\eta_2 + \eta_1} \tag{1.21}$$

The transmitted field strength is described by the transmission coefficient, T:

$$T_{12} = 1 + R_{12} = \frac{2\eta_2}{\eta_2 + \eta_1} \tag{1.22}$$

1.3.5 Wavelet Concept

In the field of GPR and TDR applications, it is assumed that an electromagnetic pulse with a finite duration in time and a specific shape is emitted. This pulse propagates in the adjacent medium and it is either directly transmitted to the receiver or it reaches the receiver after one or several reflections. The sum of all incoming pulses is the measured signal. This pulse can be called wavelet and therefore, the measured signal can be considered as a superposition of wavelets, where each wavelet travels along a different propagation path.

1.4 SFCW GPR System Parameters

The working of different blocks of an SFCW system and the description of different parameters [5] related to the SFCW GPR system are discussed in details.

The system transmits a continuous wave, where the frequency increases linearly on a fixed bandwidth with a predetermined stepped frequency. Received

signals are mixed and sampled at individual frequency steps, after which they are transferred in the time domain for pulse synthesis using inverse fast Fourier transform (IFFT) algorithm.

The frequency synthesizer block generates a signal where frequency changes f in each step. The signal will then go to the mixer and the low pass filter converts the signal from radio frequency (RF) to intermediate frequency (IF). It further travels to the ADC block resulting in a digitized waveform and finally into the IFFT block to synthesize step frequency pulses.

To understand the principle operation, the design for the system is detailed below.

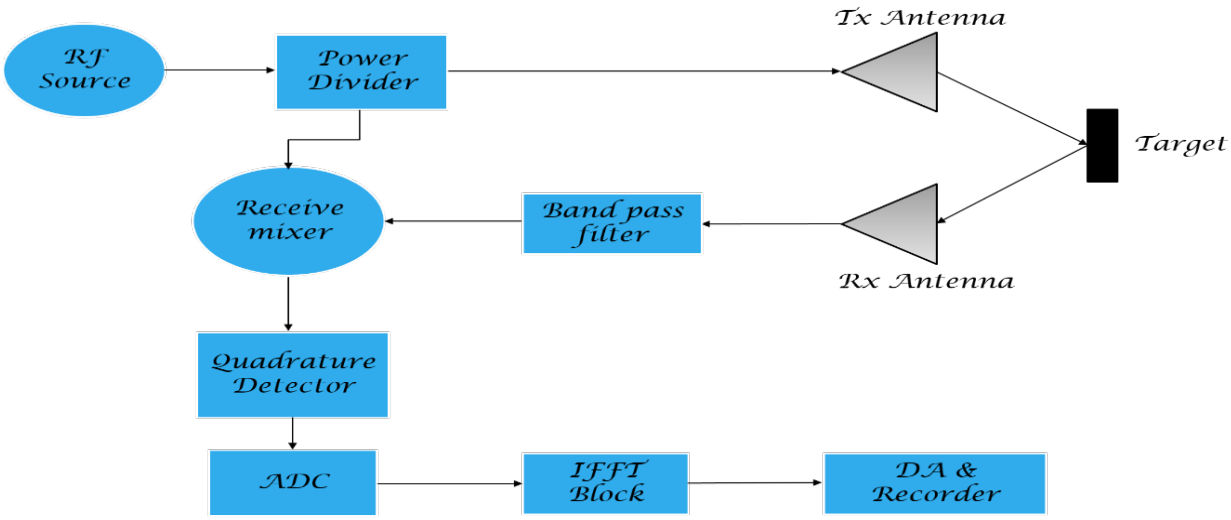

Figure 1.4: General SFCW System

The CW Generator block generates a continuous wave which is the reference frequency signal and is the same as the step frequency f at the input of the TX synthesizer block. Based on the reference frequency and digital components, TX synthesizer generates a signal that changes in each step.

SFCW waveform includes N consecutive signals which has frequency increased with fixed step frequency. The i-th frequency of TX synthesizer can be written as follows:

$$f_i = f_0 + i\Delta f\,,\ (0 \leq i \leq N-1) \tag{1.23}$$

where f_0 is the start frequency, Δf is the step frequency. Signals from CW

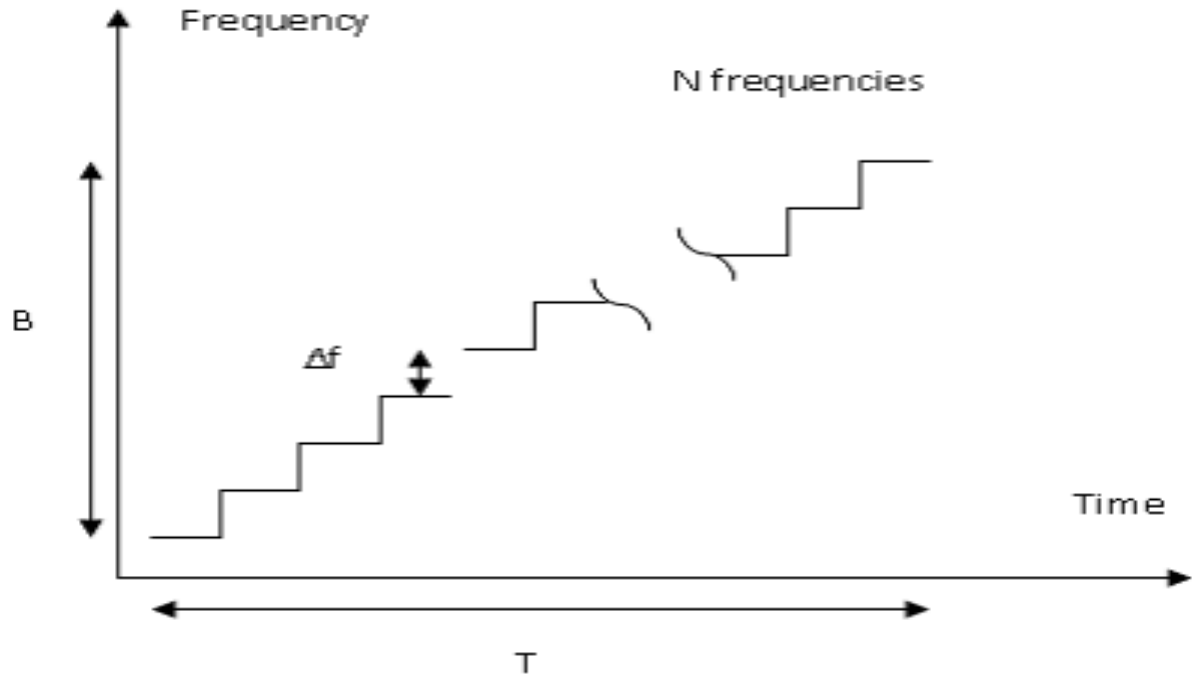

Figure 1.5: Stepped Frequency Analysis

generator also goes into the LO synthesizer block to generate the signal which has a higher frequency than the TX synthesizers frequency of Δf. The waveform of the ith signal can be expressed as the following:

$$x(t) = A_1 \cos 2\pi (f_0 + i\Delta f)t \tag{1.24}$$

When the state of the switch is off, the signal from TX synthesizer will directly go into the Mixer and then on to the other block for processing. Finally, the reference signal is synthesized by N individual intermediate frequencies f using the IFFT algorithm. When the state of the switch is on, the signal from TX synthesizer goes to the TX antenna and is emitted to the targets underground. The total loss and delay time is based on the depth and the dielectric of propagation media. The waveform of scattering signal from target to receiver can be written below:

$$y(t) = A_2 \cos 2\pi (f_0 + i\Delta f)(t - T_d) \tag{1.25}$$

where T_d is the signals time delay from the transmitter to the underground and

received at the receiver. T_d can be determined as follows:

$$T_d = \frac{2R\sqrt{\varepsilon_r}}{v_p} \tag{1.26}$$

where R is the distance from the transmitter to the target, ε_r is the dielectric parameter, and v_p the propagation velocity. The received signal is also mixed with the signal from the LO synthesizer. After processing, a signal with an intermediate frequency and phase delays caused by the transmission is obtained. Comparing it with the reference signal obtained when the state of the switch is off, the difference phase can be expressed by the equation below:

$$\begin{aligned} \phi_N &= 2\pi(f_0 + i\Delta f)\frac{2R\sqrt{\varepsilon_r}}{v_p} \\ &= \frac{4\pi f_0 R\sqrt{\varepsilon_r}}{v_p} + 2\pi\frac{\Delta f}{T}\frac{2R\sqrt{\varepsilon_r}}{v_p}iT \end{aligned} \tag{1.27}$$

where ϕ_N is the phase difference, T is the signals period which is based on the number of step frequencies and data capture time, It also determines the switching time long enough for the receiver to receive and process the reflected signal from the target. From (1.27), we can see that the first term represents a constant phase shift, and the second term represents a shift frequency during the round trip time. Assuming that fs is the shift frequency during the round trip time that we get after processing the received signal, therefore the range information of the target is based on the following equation:

$$R = \frac{v_p T}{2\Delta f\sqrt{\varepsilon_r}} f_s \tag{1.28}$$

Bandwidth β_{tol} is the sum of all the changes of every signal frequency. The relationship between the bandwidth and the frequency step Δf is as follows:

$$\beta_{total} = (n-1)\Delta f \tag{1.29}$$

And Δf must meet the following condition:

$$\frac{1}{\Delta f} \geq 2t_{\max} \tag{1.30}$$

where t_{max} is the maximum time delay during which the signal travels from the transmitter to the underground and then scatters back to receiver.

In addition, the unambiguous range of SFCW GPR is also dependent on the total bandwidth β_{total} and step size frequency Δf, can be calculated by the following formula:

$$R_{unam} = \frac{v_p}{2\beta_{total}}(n-1) \tag{1.31}$$

where n is the number of step frequencies, R_{unam} is the unambiguous range. Since the stepped frequency transmits fixed bandwidth which is essentially the total bandwidth β_{total}, the number of step frequencies is thus dependent on the size of the step frequency. Hence the equation above has a relationship with the total bandwidth β_{total} and the size of the step frequency Δf.

1.5 Different Types of GPR Scanning Mechanism

A-Scan

Time or frequency domain data acquired by a GPR antenna for one spatial localization is termed A-scan. When the velocity of propagation in the soil is known, the time vector can be transformed into distance/depth. If the targets are buried in soil, the surface contribution (which is often mixed up with the crosstalk for small antenna heights) occurs earlier and is usually much stronger than the target reflection.

B-Scan

A B-scan is the denomination of a set of A-scans gathered alongside a line that forms a two dimensional data set which schematically illustrates how GPR signal evolves with the position of the antennas with respect to the target. Reflections from targets appear as hyperbolic curves in the recorded data due to the difference in round-trip travel time between the target and the antenna system as the latter is

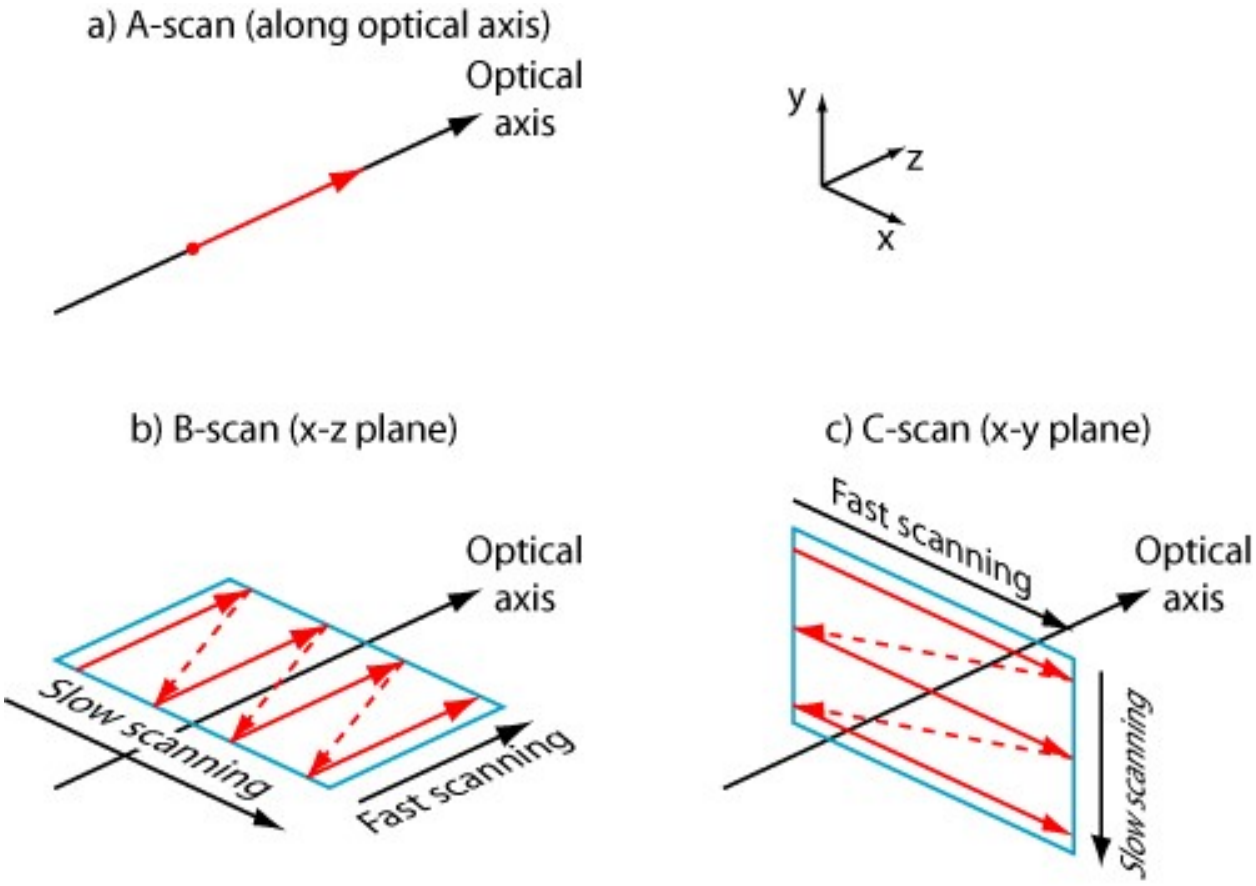

Figure 1.6: Types of GPR Scans

moved along the measurement line. The apex of the hyperbola corresponds to the antenna system located just above the target. Its shape depends on the depth of the reflector as well as the wave propagation velocity (i.e. dielectric permittivity) in soil.

C-Scan

A C-scan is represented by a horizontal slice of a number of stacked B-scans, measured by repeated line scans along the measurement plane. Three dimensional displays are basically block views of GPR traces recorded at different positions on the surface. Obtaining good three-dimensional images is of great help for interpreting images and identifying targets, which are usually easier to isolate and identify on three dimensional datasets than on conventional two dimensional profiles.

1.6 Signal Processing in GPR

GPR has gained popularity pertaining to its non-destructive, fast and hassle free nature of subsurface exploration. However in order to properly map the underground features correctly, the observer has to be experienced in figuring out the meaning of different forms of images appearing on the screen, for online as well as offline processing of data. In order to substantially reduce the complexity of the GPR images, different signal processing approaches have been put to use.

The most common and widely used signal processing method is that of IFFT. The GPR received signal is obtained in frequency domain. In order to obtain the range profile, the received signal is transformed into time domain via IFFT. This transformation helps us to understand the nature of the target medium.

Apart from IFFT, there are several subspace spectral estimation techniques, which also takes GPR frequency domain received signal as its input and gives out the direct estimation of time delays and corresponding amplitudes of the backscattered echoes from the target medium. Estimation techniques such as MUSIC, ESPRIT, etc, depend upon the signal and noise subspace of the GPR received signal. They utilize these subspace properties by applying varying techniques to obtain useful parameters with high precision.

With the help of subspace estimators, we are able to properly explore the field of layer stripping with great ease. Apart from that, very complex and time consuming optimization schemes are put to use to invert the target medium and extract their electrical properties. However, we will stick with the more resonable and efficient method of layer stripping to obtain the required parameters.

1.7 Problem Areas

Even with many benifits of GPR, it faces setbacks in some of the following cases:

- Attenuation and distortion of GPR received signal due to high conductivity.
- Unable to detect thin layered media.
- Rough surface disrupts GPR antenna movements.
- Heavy data load, storage requirements and post-processing.
- Sensitive to disturbances by other EM signals such as mobile phones, radio, etc.

1.8 Problem Definition

Study different subspace spectral estimation techniques and use two main techniques to obtain preliminary estimates of parameters of layered media which are to be further used by Layer Stripping and Full Wave Modelling approach.

1.9 Thesis Overview

CHAPTER 1: This chapter discusses the basic working principle of a Ground Penetrating Radar (GPR). Electromagnetic properties of the target medium should be known before hand in order to properly understand the working mechanism behind the propagation of an EM wave and its nature upon interacting with a target medium. Later on brief overview of the entire GPR system is defined and discussed. Of the different types of GPR, SFCW GPR is put to use in this project and a detailed working mechanism of it is described.

CHAPTER 2: This chapter deals with the spectral estimation techniques. Out of the several para-metric methods, we have discussed about MUSIC and ESPRIT models. Also in order to successfully estimate the signal subspace, we have to find

out the model order correctly. Few algorithms relating to that are described. Due to correlation between different signals, there is a need to decorrelate them. This is achieved by taking the help of different spatial smoothing algorithms.

CHAPTER 3: In this chapter we have described about layer stripping, which in general means estimating the layer properties like thickness, permittivity and conductivity. GPR method was used to estimate the electric properties by finding out the correct amplitudes of the reflected signals. Now this method may give approximate results, but accurate estimation of the electric properties is done with the help of full wave modelling technique using GMCS and NMS algorithm.

CHAPTER 4: Along with the experimental data setup, different results and their discussions are presented here.

CHAPTER 5: Conclusion alongwith future work is described here.

1.10 Summary

GPR technology is known as an advanced technology for precisely scanning and locating targets underground without destruction. Therefore, the technology can be applied to a plethora of applications. In this paper, the SFCW GPR systems have been investigated and a complete system design has been proposed backed by a simulation of the system. The system performance is evaluated with different frequency steps whilst scanning. Further, the results of implementation and measurement of designed hardware modules of SFCW GPR system were discussed. All the results prove that our designed systems are reliable and applicable.

Chapter 2

Subspace Spectral Estimation Techniques

2.1 Introduction

A Problem of Spectral Estimation: The main aim of estimating any spectral domain of a function [6] is to take a finite length signal $\{y(1), \ldots\ldots, y(N)\}$ and find out the estimate $\hat{\phi}(\omega)$ of its PSD $\phi(\omega)$, where $\omega \in [-\pi, \pi]$.

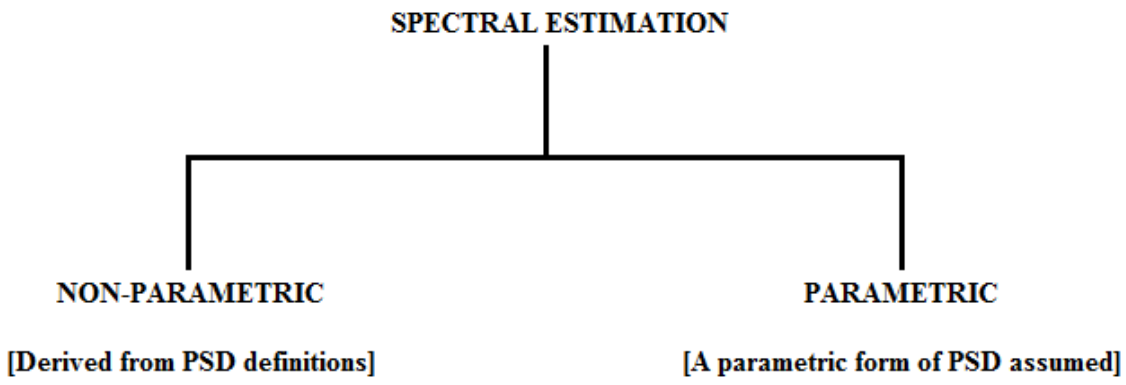

The parametric methods are used to find out the parameters making up the model into consideration. And then the spectral characteristics of the signal is extracted. In situations near to reality, the parametric methods give more precise

spectral estimates in comparison to the nonparametric techniques. But the nonparametric way of estimating PSD is still useful in situations with less knowledge of the signal to be determined.

Here we are generally concerned with the high resolution methods which implies a good ability to differentiate very alike signal components. When estimating frequency is considered, high resolution means being able to differentiate between very closely spaced frequency components. Now the parametric high resolution approach exploits the already known data structures. One can choose parametric form of expression only when the data model into consideration is explicitly detailed.

Now instead of frequency estimation, here we are going to estimate the time function of the signal in consideration. The process of estimating time function is similar to that of estimating frequency from any signal model. All the models which can estimate frequency can also estimate time function.

2.2 Sinusoidal Model

In general all the signals from different fields can be approximated by the model:

$$r(t) = s(t) + w(t) \tag{2.1}$$

Where,

$$s(t) = \sum_{k=1}^{n} \alpha_k e^{i(\omega_k t + \varphi_k)} \tag{2.2}$$

Here, $s(t)$ represents the noiseless complex sinusoidal signal. $\{\alpha_k\}$ denotes amplitudes,$\{\omega_k\}$ denotes angular frequencies and $\{\varphi_k\}$ denotes the initial phase and $\omega(t)$ is an AWGN added to the signal to make it approximate for real conditions.

Different Models for Noisy Sinusoidal Signals: In order to estimate frequency/time from noisy signals we must rely on some models [7]. The main models are as follows:

1. Nonlinear Regression Model
2. ARMA Model
3. Covariance Matrix Model

In this project we are mainly concerned with the covariance matrix model and we will be exploiting its features all the way.

2.3 Signal Model for Backscattered GPR Reflections:

Here we have considered layered homogeneous, rough less medium comprising of K layers. A single transmitter/receiver (monostatic) GPR is positioned at nadir and with the transmission of input signal, we will get K reflections from the stratified medium. The signal received combines all the reflected signals from different

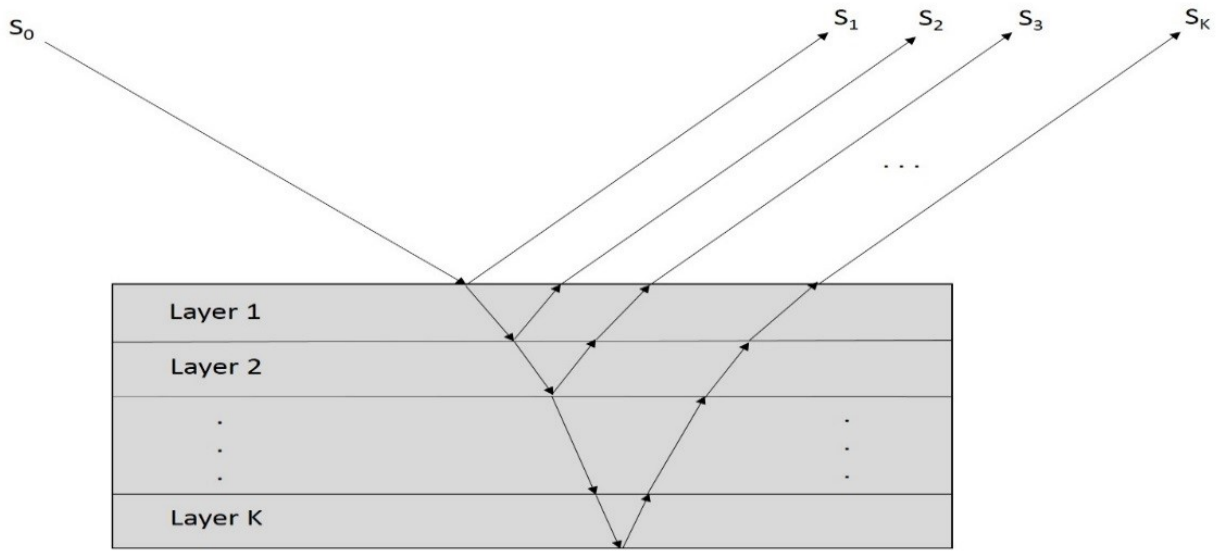

Figure 2.1: Backscattering of GPR signal in layered media

layers of media. It is represented as:

$$r(t) = \sum_{k=1}^{K} a_k e(t - T_k) + n(t) \tag{2.3}$$

Within the frequency band of operation, as a result of the low dispersion of the

target, the reflection coefficients ak does not vary the full spectrum. The signal received is thus composed of complex exponentials with an AWGN.

For the application of different spectral estimation techniques, the received signal should be defined in the frequency domain. Hence the frequency domain representation of the above equation is as follows:

$$\tilde{\mathbf{r}}(f) = \sum_{k=1}^{K} a_k \tilde{e}(f) e^{-j2\pi f T_k} + \tilde{n}(f) \tag{2.4}$$

The signal received above is represented as [7] follows:

$$\tilde{\mathbf{r}} = \boldsymbol{\Lambda A s} + \tilde{\mathbf{n}} \tag{2.5}$$

Where,

$\tilde{\mathbf{r}} = [\tilde{r}(f_1)\ \tilde{r}(f_2)\ \ldots\ldots\ \tilde{r}(f_N)]^T - Nx1$ is the resultant frequency domain vector.

$\boldsymbol{\Lambda} = diag(\tilde{\mathbf{e}}(f_1), \tilde{\mathbf{e}}(f_1),\ \ldots\ldots\ \tilde{\mathbf{e}}(f_1)) - NxN$ is a diagonal matrix with its elements as in the frequency domain of input signal.

$[\mathbf{A} = [\mathbf{m}(T_1)\ \mathbf{m}(T_2)\ \ldots\ldots\ \mathbf{m}(T_K)]$ is a mode matrix which consists of columns of vectors $\mathbf{m}(T_k) = [e^{-j2\pi f_1 T_k}\ e^{-j2\pi f_2 T_k}\ \ldots\ldots\ e^{-j2\pi f_N T_k}]^T$ which are also known as steering vectors.

$\mathbf{s} = [a_1\ a_2\ \ldots\ldots\ a_K]^T - Kx1$ is an amplitude vector of returned signals.

$\tilde{\mathbf{n}} = [\tilde{n}(f_1)\ \tilde{n}(f_2)\ \ldots\ldots\ \tilde{n}(f_N)]^T - Nx1$ is a vector of $(0, \sigma^2)$ AWGN elements.

f_n- Frequency points with equal frequency separation where the starting frequency is f_1 and Δf is the equal frequency gap.

Before we proceed with using the above equation, it should be whitened by the following vector:

$$\tilde{r}_d = \Lambda^{-1}\tilde{r} \tag{2.6}$$

Which results into the following received signal matrix: $\mathbf{r} = \mathbf{AS} + \mathbf{n}$

Where,

r: whitened received signal

n: whitened AWGN vector

2.4 Subspace Estimation Techniques

2.4.1 Spectral MUltiple SIgnal Classification (MUSIC) :

Here we define a cost function which measures the inverse of the orthogonality between the signal and noise subspace of the received signal. A peak in the pseudo spectrum of the MUSIC will take place in the time delay which gives the location of the target.

The MUSIC algorithm is used to estimate the GPR signal time delay using the following steps:

Step 1: Evaluate R from the previous section.

$$\begin{aligned} \mathbf{R} &= \mathbf{ASA}^H + \sigma^2\mathbf{I}, \\ &= \mathbf{R}_s + \sigma^2\mathbf{I}, \end{aligned} \tag{2.7}$$

Where,

$$\mathbf{R}_s = \mathbf{ASA}^H \tag{2.8}$$

$$\mathbf{A} = \begin{pmatrix} E|a_1|^2] & 0 & 0 \\ 0 & E|a_2|^2] & 0 \\ 0 & 0 & E|a_M|^2] \end{pmatrix} \tag{2.9}$$

Step 2: The signal covariance matrix, *Rs*, is clearly a N N matrix with rank M. It therefore has NM eigenvectors corresponding to the zero eigenvalue. Let $\mathbf{q}_m$ be

such an eigenvector. Therefore,

$$\begin{aligned} &\mathbf{R}_s\mathbf{q}_m = \mathbf{A}\mathbf{S}\mathbf{A}^H\mathbf{q}_m = 0, \\ &\Rightarrow \mathbf{q}_m\mathbf{A}\mathbf{S}\mathbf{A}^H\mathbf{q}_m = 0, \\ &\Rightarrow \mathbf{A}^H\mathbf{q}_m = 0 \end{aligned} \tag{2.10}$$

Step 3: Last expression suggests that the signal steering vectors are orthogonal to the noise vectors. This is the base of MUSIC algorithm. Hence, the MUSIC pseudo spectrum can be shown as:

$$P_{MUSIC}(t) = \frac{1}{\sum_{m=1}^{N-M} \left|a^H(t)\mathbf{q}_m\right|^2} = \frac{1}{a^H(t)\mathbf{Q}_n{\mathbf{Q}_n}^H a(t)} = \frac{1}{\left\|{\mathbf{Q}_n}^H a(t)\right\|^2} \tag{2.11}$$

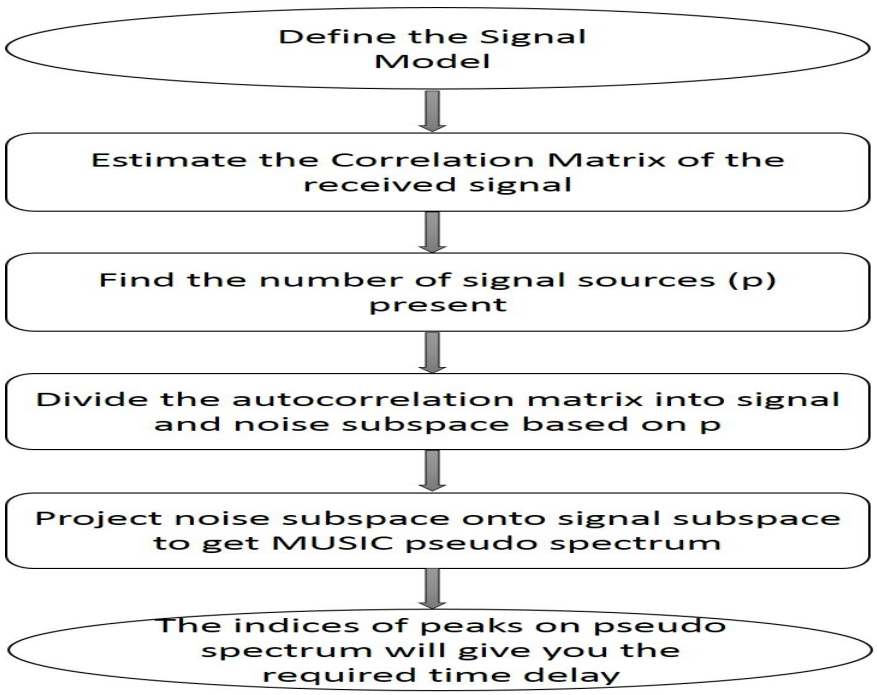

Figure 2.2: Flowchart depicting the working of Spectral MUSIC algorithm

2.4.2 Root MUltiple SIgnal Classification (R-MUSIC):

The accuracy of MUSIC pseudo spectrum is limited. Hence, we have opted to more rea-sonable method of estimating the time delays. A Model Based Parameter

Estimation (MBPE) named Root MUSIC is employed. It works as the polynomial version of the spectral MUSIC.

The Root MUSIC algorithm is used to estimate the GPR signal time delay using the following steps:

Step 1: Let us define:

$$z = e^{-j2\pi\Delta f\tau} \tag{2.12}$$

$$s(\tau) = [1,\ z,\ z^2,\ .....\ , z^{N-1}]^T \tag{2.13}$$

$$\Rightarrow q_m^H s = \sum_{n=0}^{N-1} q_{mn}^* z^n = q_m(z) \tag{2.14}$$

i.e., the final expression gives a polynomial in z which leads us to finding the roots of the polynomial.

Step 2: To find the polynomial whose roots we wish to evaluate, we use

$$\begin{aligned} P_{MUSIC}^{-1}(\tau) &= s^H(\tau) Q_n Q_n^H s(\tau) \\ &= s^H(\tau) C s(\tau) \end{aligned} \tag{2.15}$$

$$where,\ C = Q_n Q_n^H \tag{2.16}$$

$$\Rightarrow P_{MUSIC}^{-1}(\tau) = \sum_{m=0}^{N-1} \sum_{n=0}^{N-1} z^{(n-m)} C_{mn} \tag{2.17}$$

The above expression can be replaced by

$$\begin{aligned} \Rightarrow P_{MUSIC}^{-1}(\tau) &= \sum_{l=-(N-1)}^{(N+1)} C_l z^l, \\ C_l &= \sum_{n-m=l} C_{mn} \end{aligned} \tag{2.18}$$

i.e., C_l is the sum of the elements of C on the nth diagonal. The zeros of $P_{MUSIC}^{-1}(\tau)$ come in pairs. Here, one zero is within the unit circle and the other outside.

Step 3: We obtain the time delays using the following expression:

$$\tau_m = \frac{angle(z_m)}{(-2\pi\Delta f)},\ m = 1,\ 2,\ .....\ ,M \tag{2.19}$$

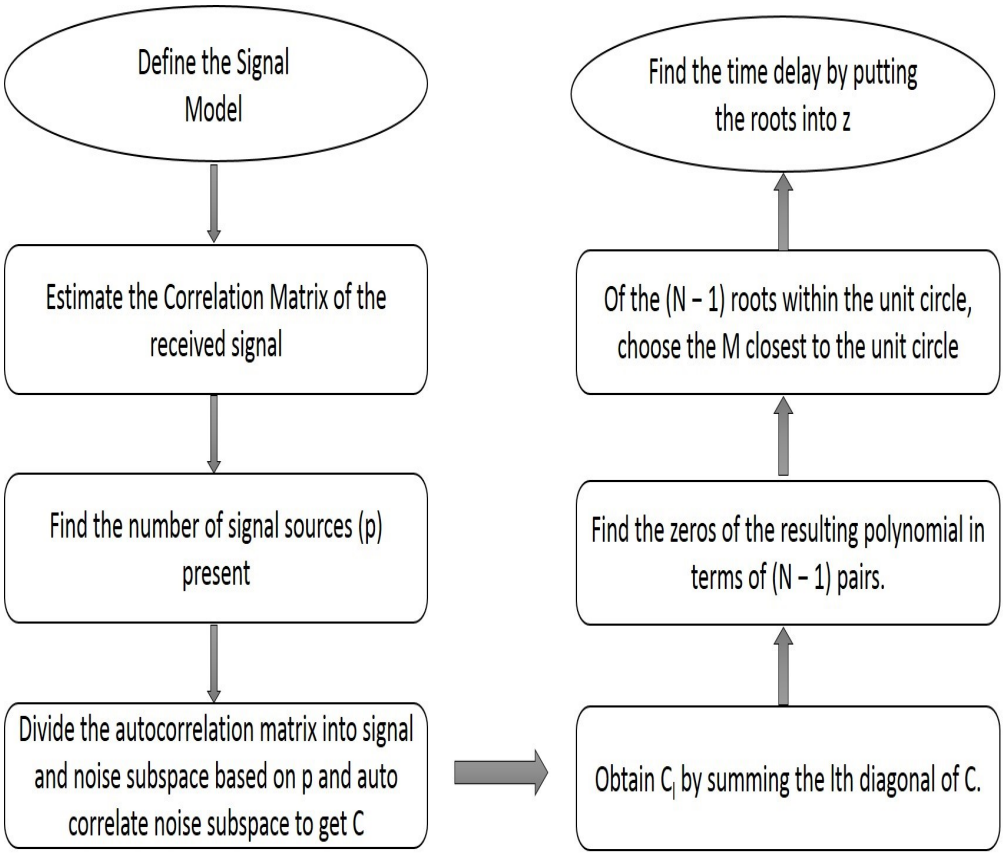

Figure 2.3: Flowchart depicting the working of Root MUSIC algorithm

2.4.3 Estimation of Signal Parameters via Rotational Invariance Technique (ESPRIT):

ESPRIT feeds on the information of one signal being at the same phase shift from the previous. We can process the ESPRIT method to obtain the time delay of GPR reflected signals using Least Squares (LS) and Total Least Squares (TLS) methods.

We know that the correlation matrix depends on S, given by:

$$[\mathbf{S} = \begin{pmatrix} 1 & 1 & \cdots & 1 \\ z_1 & z_2 & \cdots & z_M \\ \vdots & \vdots & \ddots & \vdots \\ z_1^{N-2} & z_2^{N-2} & \cdots & z_M^{N-2} \\ z_1^{N-1} & z_2^{N-1} & \cdots & z_M^{N-1} \end{pmatrix} \tag{2.20}$$

Let us break this matrix into two separate matrices of S0 and S1, given by:

$$\mathbf{S}_0 = \begin{pmatrix} 1 & 1 & \cdots & 1 \\ z_1 & z_2 & \cdots & z_M \\ \vdots & \vdots & \ddots & \vdots \\ z_1^{N-2} & z_2^{N-2} & \cdots & z_M^{N-2} \end{pmatrix} \mathbf{S}_1 = \begin{pmatrix} z_1 & z_2 & \cdots & z_M \\ \vdots & \vdots & \ddots & \vdots \\ z_1^{N-2} & z_2^{N-2} & \cdots & z_M^{N-2} \\ z_1^{N-1} & z_2^{N-1} & \cdots & z_M^{N-1} \end{pmatrix}$$

It should be noted that $\mathbf{S}_1 = \mathbf{S}_0\mathbf{\Phi}$, where $\mathbf{\Phi}$ is the M x M matrix given by:

$$\mathbf{\Phi} = \begin{pmatrix} z_1 & 0 & \cdots & 0 \\ 0 & z_2 & \cdots & 0 \\ \vdots & \vdots & \ddots & \vdots \\ 0 & 0 & \cdots & z_M \end{pmatrix} \tag{2.21}$$

The above matrix can be called as rotational matrix. Its elements tells us about the phase shift from one signal to the next. Thus, in order to estimate the time delay, we have to find out $\mathbf{\Phi}$.

The steering vectors in S belong to the signal subspace matrix *Qs*. Therefore, **S0** and **S1** are related to each other by a matrix C such that,

$$\mathbf{Q}_s = \mathbf{SC} \tag{2.22}$$

Defining **Q0** and **Q1** similarly as **S0** and **S1**, we get

$$\begin{aligned} \mathbf{Q}_0 &= \mathbf{S}_0\mathbf{C} \\ \mathbf{Q}_1 &= \mathbf{S}_1\mathbf{C} = \mathbf{S}_0\mathbf{\Phi}\boldsymbol{C} \end{aligned} \tag{2.23}$$

Let us consider,

$$\mathbf{Q}_1\mathbf{C}^{-1}\mathbf{\Phi}^{-1}\mathbf{C} = \mathbf{S}_0\mathbf{\Phi}\boldsymbol{C}\mathbf{C}^{-1}\mathbf{\Phi}^{-1}\mathbf{C} = \mathbf{S}_0\mathbf{C} = \mathbf{Q}_0 \tag{2.24}$$

Now let,

$$\begin{aligned} \mathbf{\Psi}^{-1} &= \mathbf{C}^{-1}\mathbf{\Phi}^{-1}\mathbf{C} \\ \Rightarrow \mathbf{Q}_1\mathbf{\Psi}^{-1} &= \mathbf{Q}_0 \end{aligned} \tag{2.25}$$

$$\therefore \mathbf{Q}_1 = \mathbf{Q}_0\mathbf{\Psi} \tag{2.26}$$

1. Least Squares ESPRIT: Here we need to minimize the difference between $\mathbf{Q}_0\mathbf{\Psi}$ and $\mathbf{Q}_1$.

   Upon minimizing [8], we get

   $$\hat{\mathbf{\Psi}}_{LS} = \mathbf{C}^{-1}\mathbf{\Phi}\boldsymbol{C} \tag{2.27}$$

   Where, $\mathbf{\Phi}$ is the diagonal matrix of the eigenvalues of $\mathbf{\Psi}$. Then we have to find the eigenvalues of $\hat{\mathbf{\Psi}}$, which upon equating the angle of z, will give us the time delay estimates.

2. Total Least Squares ESPRIT: Both **Q0** and **Q1** are found from the SVD of noise correlation matrix. Hence, errors are prone to this technique. TLS-ESPRIT is used to correct the errors. We first modify the received signal as follows:

   $$\mathbf{X} = \begin{pmatrix} r_{01} & r_{11} & \cdots & r_{(N-1)1} \\ r_{02} & r_{12} & \cdots & r_{(N-1)2} \\ \vdots & \vdots & \ddots & \vdots \\ r_{0K} & r_{1K} & \cdots & r_{(N-1)K} \end{pmatrix} \tag{2.28}$$

   Upon performing SVD operation on $\mathbf{X}$, gives us $\mathbf{X} = \boldsymbol{U}\mathbf{\Sigma}\mathbf{Q}^H$. Here $\mathbf{Q}$ is the matrix of eigenvectors of X^HX, which is directly related to the correlation matrix $\mathbf{R}$. Now we have to partition the $\mathbf{V}$ matrix into four M x M matrices.

We thus get the following matrix,

$$\mathbf{V} = \begin{pmatrix} \mathbf{V}_{11} & \mathbf{V}_{12} \\ \mathbf{V}_{21} & \mathbf{V}_{22} \end{pmatrix} \tag{2.29}$$

Thus, we get the estimates as

$$\hat{\mathbf{\Psi}}_{TLS} = -\mathbf{V}_{12}\mathbf{V}_{22}^{-1} \tag{2.30}$$

Then we have to find the eigenvalues of $\hat{\mathbf{\Psi}}$, which upon equating the angle of z, will give us the time delay estimates.

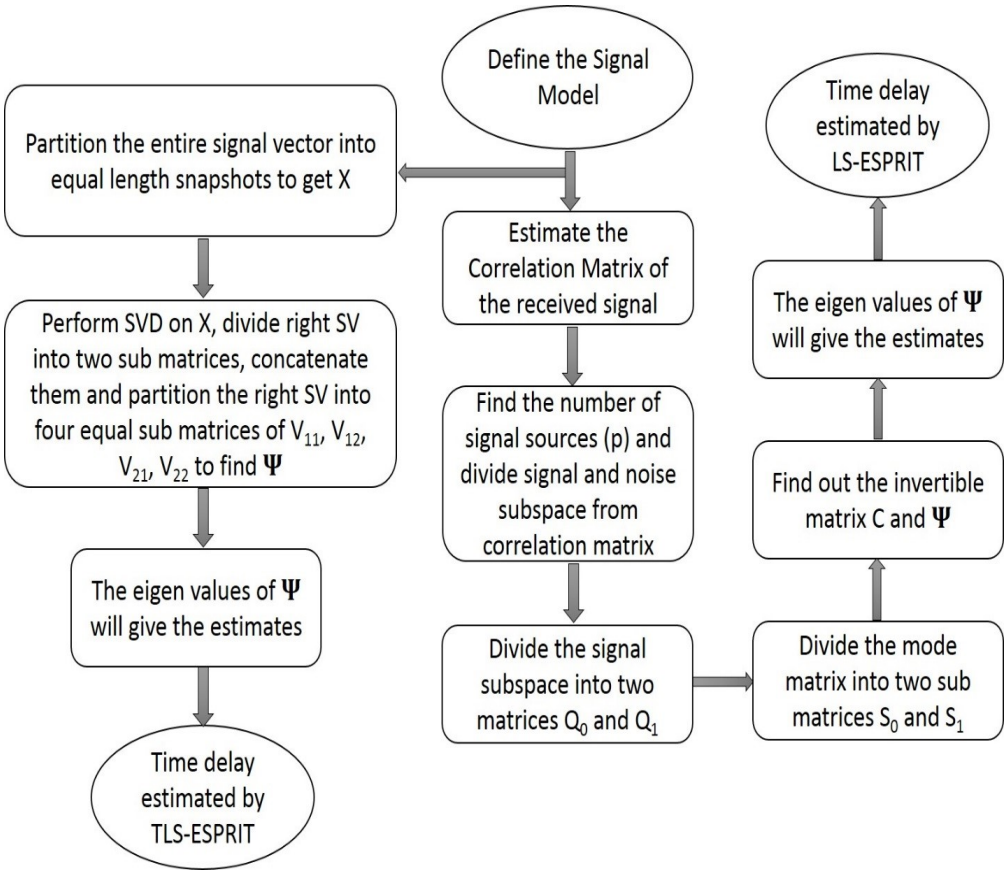

Figure 2.4: Flowchart depicting the working of LS and TLS ESPRIT algorithm

2.5 Signal Number Estimation

Number of echo signal received on the receiver antenna plays an important part in the proper functioning of different estimation algorithms. For high SNR, the number of received signals can be approximated with ease. But in real life conditions, SNR is usually low and there is a fine distinction between required signal and noise. Hence to judge signal number correctly, a good estimation criterion is needed, which can distinguish between signal and noise subspace.

Two main techniques [9] are mentioned which can correctly find out the number of signals. We have to find the order of eigenvalues in noise subspace. In ideal case, they are same and easy to identify. But in reality, they are unequal. We therefore have to find an estimate of the degree of how close the eigenvalues are. Let us suppose we take M snapshots of original data and assume there are k signals.

Let us define the measure of closeness of the noise Eigen values λ as:

$$L(k) = -\frac{M(N-1)}{(N-k)}\log(\prod_{n=k+1}^{N}\lambda_n) + M(N-1)\log(\frac{1}{N-k}\sum_{n=k+1}^{N}\lambda_n) \qquad (2.31)$$

Where, $k \in \{0, 1, ..., K-1\}$

Using L, we define two criteria as under.

1. Minimum Descriptive Length Criteria (MDL):Similarly, here also result is found for the value of k which results in minimum value of the criteria:

$$MDL(k) = -\frac{M(N-1)}{(N-k)}\log(\prod_{n=k+1}^{N}\lambda_n) + M(N-1)\log(\frac{1}{N-k}\sum_{n=k+1}^{N}\lambda_n) + \frac{1}{2}k(2N-k)log \qquad (2.32)$$

   However, this technique is unable to give sufficiently good results. Hence another method is applied to give better results.

2. Malinowskis Method: Malinowski used Empirical Indicator Function de-

fined by

$$EIF(p) = \frac{\left(\sum_{l=p+1}^{N} \lambda_l \right)^{1/2}}{N^{1/2}(N-p)^{3/2}} \tag{2.33}$$

The model order estimate is found out by the index which gives the minimum value of the function EIF.

2.6 Various Smoothing Techniques

There are many situations when more than one signal is received by the same receiver or different receivers located very close to each other. In such circumstances, there is a great deal of possibility for increased correlation between the signals. As a result we are unable to separate each signal efficiently. This leads to a drop in the efficiency of high-resolution techniques. To counter this disability, Evans et al., and later by Shan et al., suggested spatial smoothing techniques. These techniques take different independent snapshots of the data vector, evaluate their covariance matrix and apply them depending on the type of spatial smoothing technique applied.

There are mainly two types of spatial smoothing techniques used:

1. Forward Spatial Smoothing Technique: Here the equal subbands are selected sequentially from one end to the other, auto correlated, and then averaged.

2. Forward-Backward Spatial Smoothing Technique: Here the subbands are selected sequentially from both ends, one at a time. They are autocorrelated and then averaged together.

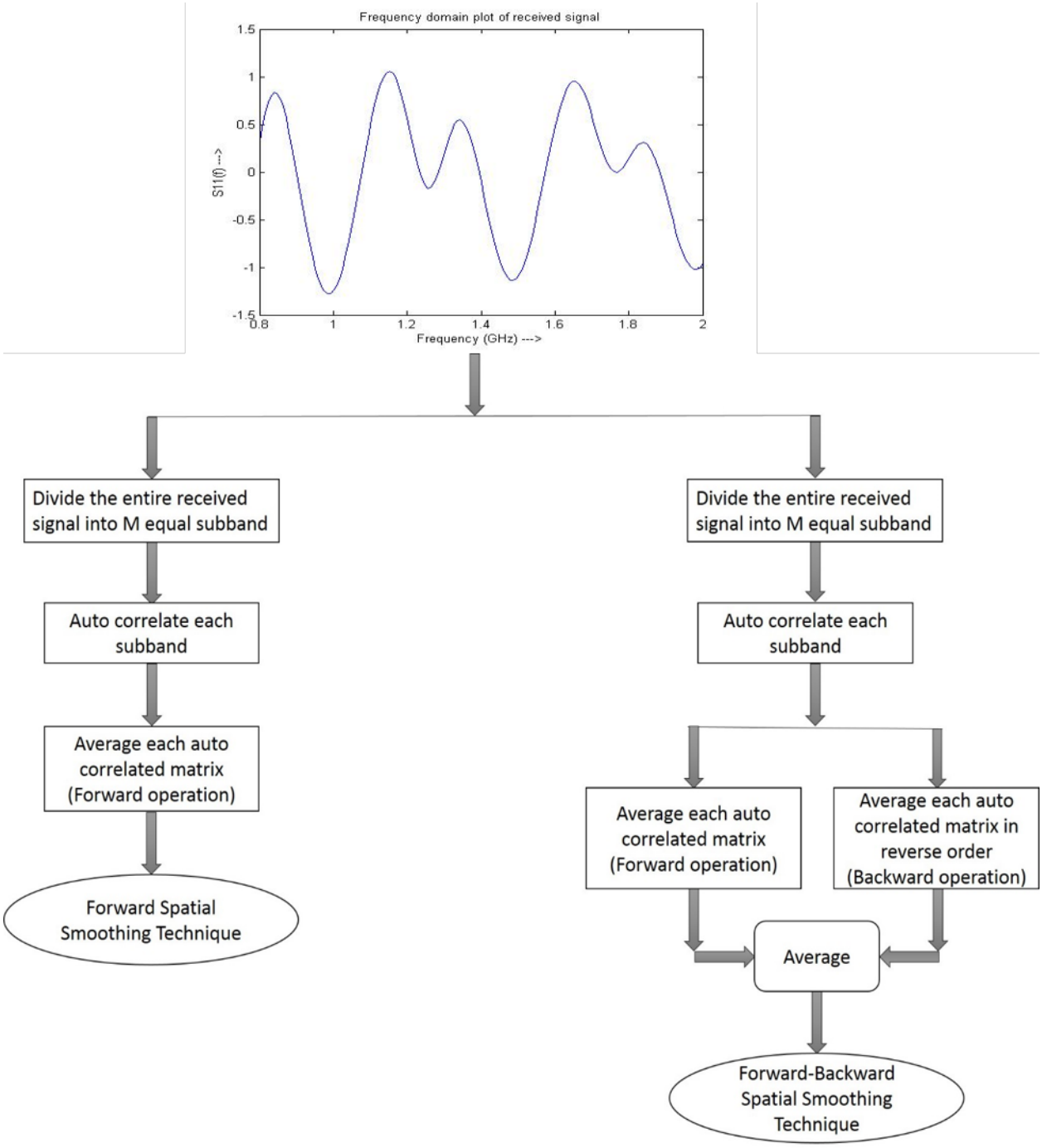

Figure 2.5: Forward and Forward-backward Spatial Smoothing Approach

If we suppose that is divided into M equal subbands of length N, then the set of subbands can be represented as $[\mathbf{r}_1, \mathbf{r}_2, ..., \mathbf{r}_M]$, where $\mathbf{r}_k$ is the kth subband with $k = 1, 2, ..., M$.

Autocorrelation of each subband can be represented by

$$\mathbf{R}_k = E[\mathbf{r}_k \mathbf{r}_k{}^H] \tag{2.34}$$

1. Forward Spatial Smoothing Technique: Here the function $R_k \forall k$ is forward averaged to give the following expression:

$$\mathbf{R}_f = \frac{1}{M} \sum_{k=1}^{M} (\mathbf{r}_k \times \mathbf{r}_k{}^H) \tag{2.35}$$

2. Forward Backward Spatial Smoothing Technique: Here along with forward approach, we need to find out the backward approach. Autocor-relation with backward approach is defined as:

$$\mathbf{R}_b = J\mathbf{R}_f{}^* J \tag{2.36}$$

Where, J is eye function with ones on the anti diagonal of the matrix with (NxN) size. Final result is obtained by averaging the forward and backward smoothing matrices. The resultant function is defined as:

$$\mathbf{R}_{fb} = (\mathbf{R}_f + \mathbf{R}_b)/2 \tag{2.37}$$

2.7 Summary

There are many subspace spectral estimation techniques, of which we have decided to work with Root-MUSIC and TLS-ESPRIT. These two methods have proved to be superior than the rest of the estimation techniques. In order to properly estimate time delays using the estimation algorithms, the number of signal sources are to be defined correctly. We have used two order estimation techniques and will compare them later to find out the better one. Also different spatial smoothing algorithms have been put to use to decorrelate the correlated or coherent signal sources.

Chapter 3

GPR Signal Modelling for Layered Media

3.1 Introduction

Estimation of layered media parameters is a thriving area of research. Inversion method for layered media are generally classified into : Time domain and Frequency domain [10]. Common Middle Point (CMP) method requires the echoes of the layers to be distinguishable in time domain. In case of frequency domain algorithms, a forward model is to be made and then the required parameters are obtained when the modelled and measured spectrum matches with each other with minimum error. Lambot et al. established objective function based on Green function for inversion of thickness and electric parameters [11]. Now this full wave inversion method provide accurate estimates but are complex and not realizable in outdoor working conditions. Whereas, layer stripping approach extracts the parameters of the layers one by one from the stack with great speed. Its accuracy may not be as good compared to full wave inversion method, but its ability to provide results in mobile GPR working conditions, such as tracking of road pavements, gives it an upper hand.

3.2 Plane Wave Model

Let us suppose we have single layered medium with a PEC as its boundary as shown below:

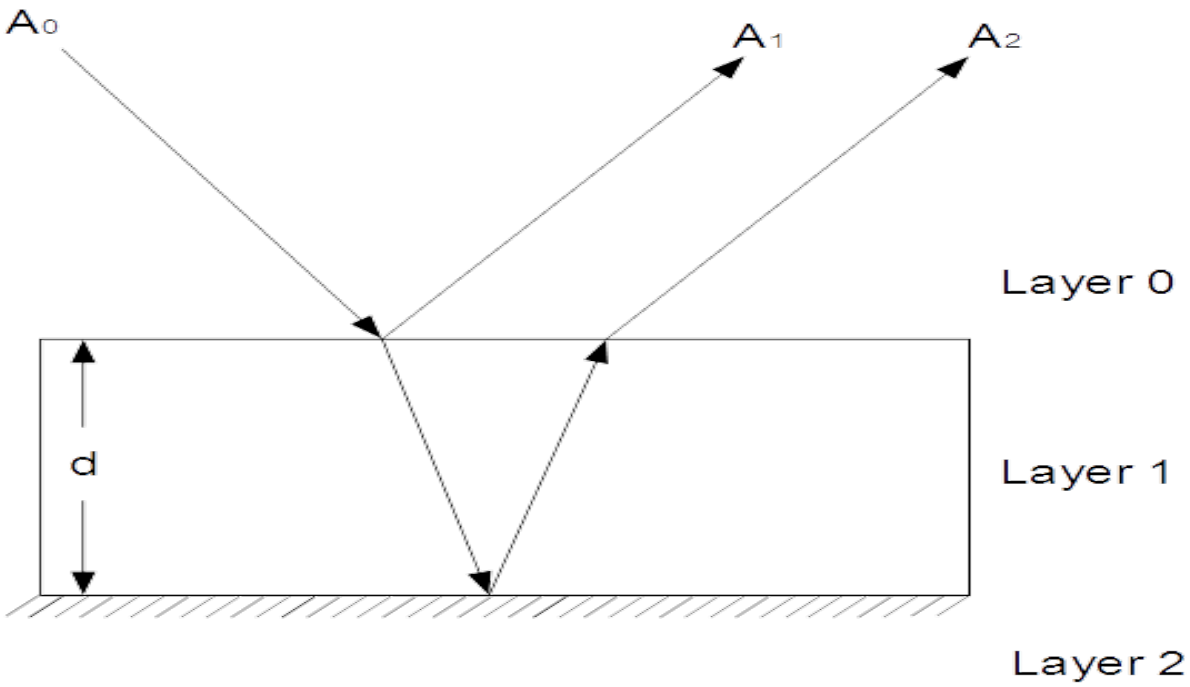

Figure 3.1: Three layered target medium

At the interface the amplitudes of the incident ray A0 and the reflected ray A1 are related by the reflection coefficient r01 [12] as follows:

$$A_1 = r_{01}A_0 \tag{3.1}$$

The ray reflected at the medium/PEC interface is expressed likewise

$$A_2 = t_{01}r_{12}t_{10}A_0e^{-2\alpha d} \tag{3.2}$$

Where A0 is the source amplitude and A2 is the amplitude of the transmitted ray at the air/media interface. is the attenuation coefficient and 2d the two-way travel distance. The reflection and transmission coefficients are given as, rab, tab,

and tba; where the indices a stand for 1st media, b for 2nd media.

$$r_{ab} = \frac{\sqrt{\varepsilon_a} - \sqrt{\varepsilon_b}}{\sqrt{\varepsilon_a} + \sqrt{\varepsilon_b}} \tag{3.3}$$

$$t_{ab} = \frac{2\sqrt{\varepsilon_a}}{\sqrt{\varepsilon_a} + \sqrt{\varepsilon_b}} \tag{3.4}$$

$$t_{ba} = \frac{2\sqrt{\varepsilon_b}}{\sqrt{\varepsilon_a} + \sqrt{\varepsilon_b}} \tag{3.5}$$

Now equation of rab is used when we dont consider any internal reflections. But in real life scenario, multiple reflections occur between two interfaces of layered medium. So a general term which represents the overall reflection coefficients between any number of interfaces, is called Global Reflection Coefficient.

From equation (3.2) we find that:

$$\frac{A_2}{A_0} = t_{01} r_{12} t_{10} e^{-2\alpha d} \tag{3.6}$$

We know that,

$$t_{01} = 1 + r_{01} \tag{3.7}$$

$$t_{10} = 1 - r_{01} \tag{3.8}$$

$$\therefore t_{01} t_{10} = 1 - {r_{01}}^2 \tag{3.9}$$

Replacing equation 3.9 in equation 3.2, we get

$$\frac{A_2}{A_0} = r_{12}(1 - {r_{01}}^2) e^{-2\alpha d} \tag{3.10}$$

$$\Rightarrow \tilde{r}_{12} = r_{12}(1 - {r_{01}}^2) e^{-2\alpha d} \tag{3.11}$$

Now on generalizing the above eq, we get the global reflection coefficient for ith interface as

$$\tilde{r}_{i,i+1} = r_{i,i+1} \prod_{j=0}^{i-1} (1 - {r_{j,j+1}}^2) \prod_{j=1}^{i} \exp(-2\alpha_j d_j) \tag{3.12}$$

Here, α_j represents the attenuation suffered by EM wave for jth layer and represents the width of jth layer and d_j. Similarly the Total Reflection Coefficient is obtained by superimposing all the global reflection coefficients from each interface of the layered media.

3.3 Full Wave Model

3.3.1 VNA-Antenna-ground subsurface modelling

The monostatic UWB SFCW GPR uses Vector Network Analyzer (VNA) for the measurement. The GPR signal is modelled based on the complex reflection coefficient S11 () measurement at the VNA port [13]. The VNA, antenna and subsurface are modelled as linear systems in series and parallel as given below:

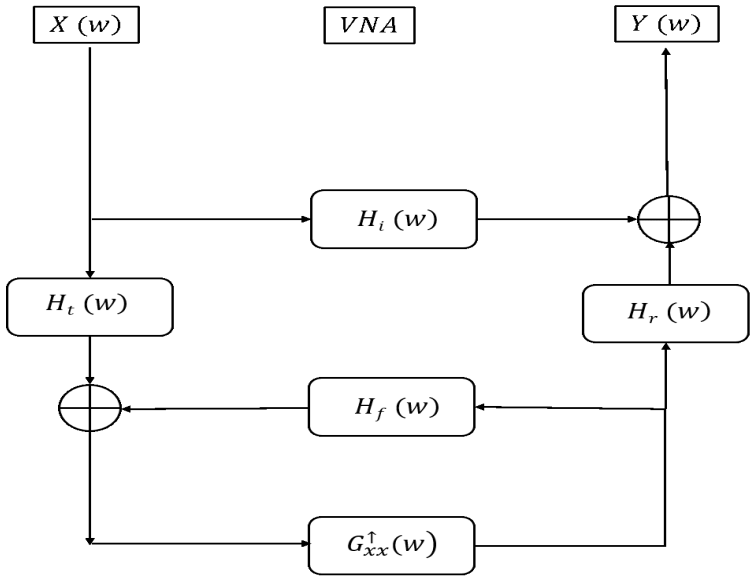

Figure 3.2: Block diagram representing the VNAantennamultilayered medium system

By applying Massons gain formula we get

$$S_{11}(\omega) = \frac{Y(\omega)}{X(\omega)} = H_i(\omega) + \frac{H_t(\omega)G^{\uparrow}_{xx}(\omega)H_r(\omega)}{1 - H_f(\omega)G^{\uparrow}_{xx}(\omega)} \tag{3.13}$$

where $X(\omega)$ is the transmitted signal and $Y(\omega)$ is the received signal at the VNA reference plane; Hi(w) is the return loss of the antenna, $Ht(\omega)$ is the transmit transfer function of the antenna, $Hr(\omega)$ is the receive transfer function of the antenna, and $Hf(\omega)$ represents the feedback loss transfer function. $G_{xx}^{\uparrow}(\omega)$ is the transfer function representing the air-subsurface systems. This is also called as Greens function of the air-subsurface system. All these reflection and transfer functions can be measured by the calibration testing process on known model configurations of ground. In this case the measurements are taken with antenna placed at different heights on a metal sheet.

3.3.2 Modelling air-subsurface with Greens function

Here the air-ground surface is modelled as an N horizontal layered medium separated by N-1 interfaces as illustrated in the figure below.

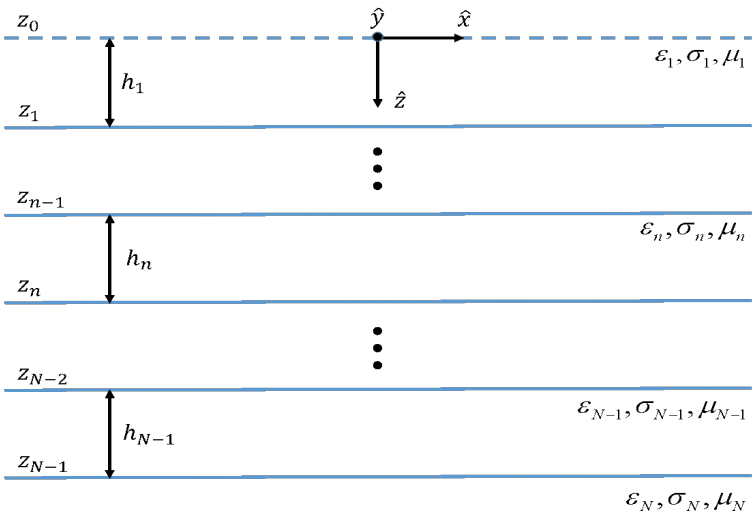

Figure 3.3: Model configuration of N-layered medium with a point source

Any single nth layer is homogeneous and is characterized by permittivity (ε_n), conductivity (σ_n) and thickness (h_n). The permeability (μ_n) is assumed to be free space value (μ_0). The Greens function ($G_{xx}^{\uparrow}$) here is the solution of Maxwells equation for the multilayered media for the unit source. The source and receiver point is located at the upper half space, at the origin O of the coordinate system. The radiating part of the horn antenna is assumed to be an infinitesimal horizontal

x -directed electric dipole (second subscript in $G_{xx}^{\uparrow}$) and the receiving part of the antenna is denoted by measuring the horizontal x -directed part (first subscript in $G_{xx}^{\uparrow}$) of the backscattered electric field (up arrow in $G_{xx}^{\uparrow}$). The effect of the soil roughness is neglected according to the Rayleigh criterion.

Now following the approach of Lambot et al. the spatial domain Greens function at the source point ((x, y, z) = 0) is obtained from the spectral domain Greens function as

$$G_{xx}^{\uparrow}(0,\omega) = \frac{1}{4\pi}\int_{0}^{+\infty} \tilde{G}_{xx}^{\uparrow}(k_\rho,\omega)dk_\rho \tag{3.14}$$

The integration variable k_ρ is a spectral parameter. The analytical expression of the Greens function in the spectral domain can be derived and its final form is given below

$$\tilde{G}_{xx}^{\uparrow}(k_\rho,\omega) = \left[R_n^{TM}\frac{\Gamma_n}{\eta_n} - R_n^{TE}\frac{\zeta_n}{\Gamma_n}\right] e^{-2\Gamma_n h_n} \tag{3.15}$$

where n = 1 for single layered ground media, R_n^{TM} is the transverse magnetic global reflection coefficient and R_n^{TE} is the transverse electric global reflection coefficient accounting for all reflections from the multilayered interfaces. Γ_n is the vertical wave number of the n-th layer defined as $\Gamma_n = \sqrt{k_\rho^2 + \zeta_n\eta_n}$, $\zeta_n = i\omega\mu_n$ and $\eta_n = \sigma_n + i\omega\varepsilon_n = j\omega\varepsilon_{e,n}$.

3.3.3 Model Inversion

The estimation of subsurface material parameters by the inversion of forward modelling is a non-linear problem. We need to find out the vector b= [ε_n, σ_n, h_n] of parameters so that the objective function ϕ_b is minimized. If observation errors are independent zero mean stationary Gaussian process and there is no prior information on parameters, the maximum likelihood approach reduces to the weighted least-squares problem. Therefore the objective function can be defined as following

$$\phi(b) = \left|G_{xx}^{\uparrow *}(\omega) - G_{xx}^{\uparrow}(\omega,b)\right|^{T}\frac{1}{\sigma^2}\left|G_{xx}^{\uparrow *}(\omega) - G_{xx}^{\uparrow}(\omega,b)\right| \tag{3.16}$$

Where, $G_{xx}^{\uparrow *}(\omega)$ are the vectors containing measured and $G_{xx}^{\uparrow}(\omega, b)$ are the vectors containing simulated response function of the multilayered medium, and σ^2 is the error variance. The objective function $\phi(b)$ is highly non-linear and has got multiple minima over the multi-dimensional parameter vector space. Here a GA based hybrid algorithm is implemented in Matlab to estimate the soil parameters. The number of parameters need to be optimized for a single layered ground media are five i.e. height of the antenna from the sand surface ($h0$), sand layer thickness ($h1$), relative dielectric constant (ε_{r1}), static conductivity (σ_{01}) and conductivity variation coefficient (α). The efficiency of GA based technique depends on defining initial parameter vector and its range of variation. Here the initial values of parameters are calculated based on GPR processing by the surface reflection coefficient method.

3.4 Layer Stripping Approach

3.4.1 Introduction

Even with the presence of different inverse modelling schemes, we are bound to look for alternative methods for exploration of subsurface. This is caused by the complexity and time consuming nature of the inversion methods. As a result, way is paved for a more practical and comparatively efficient method of Layer Stripping approach. Here, amplitudes and timing information of the GPR received signals are put to use to strip the layer parameters one by one from the top.

3.4.2 Reflection method used for Layer Stripping

Reflection coefficient is determined from this approach. Few parameters are taken into consideration: (1) Antennas are placed in free space above soil, (2) The EM waves are considered to be plane waves, (3) Distortion due to antenna is minimum, (4) Water content is assumed to be very less, (5) Soil is assumed non-magnetic, and (6) Permittivity is frequency independent.

For normal incidence, reflection coefficient can be represented from [14] as:

$$R = \frac{1 - \sqrt{\varepsilon_r}}{1 + \sqrt{\varepsilon_r}} \tag{3.17}$$

Where, ε_r is Relative Dielectric Permittivity (RDP) of the soil. Hence the soil RDP can be expressed as:

$$\varepsilon_r = \left(\frac{1-R}{1+R}\right)^2 \tag{3.18}$$

Reflection coefficient is usually found out by comparing the reflections from the interfaces with that of a PEC from the same interface. Hence the dependence is expressed as:

$$\frac{R}{R_{PEC}} = \frac{\frac{E_s}{E_i}}{\frac{E_{s,PEC}}{E_i}} \tag{3.19}$$

Here *RPEC* = -1, hence the above equation reduces to:

$$R = -\frac{E_s}{E_{s,PEC}} = -\frac{A}{A_{PEC}} \tag{3.20}$$

3.4.3 Estimation of Static Dielectric Constant from Reflection Amplitudes

In order to gain maximum advantage, we should utilize the GPR reflected signals directly. Since the layer thickness is directly related to the amplitudes and electric permittivity, we can estimate the permittivity by accurately formulating the different amplitudes of received signals [15] with respect to the incoming signal. Thus we can introduce the layer thickness information:

$$d = \frac{c\Delta t}{2\sqrt{\varepsilon_r}} \tag{3.21}$$

into the expression of the relative reflection amplitude *An* given by equation

$$A_n = \frac{\sqrt{\varepsilon_{r,n}} - \sqrt{\varepsilon_{r,n+1}}}{\sqrt{\varepsilon_{r,n}} + \sqrt{\varepsilon_{r,n+1}}} \left[\prod_{i=0}^{n-1}(1-\gamma_i^2)\right] e^{-\eta_0 \sum_{i=0}^{n} \frac{\sigma_i d_i}{\sqrt{\varepsilon_{r,i}}}} \tag{3.22}$$

Which reduces the above equation to the following:

$$A_n = \frac{\sqrt{\varepsilon_{r,n}} - \sqrt{\varepsilon_{r,n+1}}}{\sqrt{\varepsilon_{r,n}} + \sqrt{\varepsilon_{r,n+1}}} \left[\prod_{i=0}^{n-1} (1-\gamma_i^2) \right] e^{-\eta_0 \sum_{i=0}^{n} \frac{\sigma_i t_i c}{2\varepsilon_{r,i}}} \tag{3.23}$$

where $\varepsilon_{r,n}$,σ_n, and tn are, respectively, the dielectric constant, conductivity, and two-way travel time at layer n and γ_n is the reflection coefficient at layer interface n.

Upon substituting the values of permittivity for free space, we get the permittivity for the first layer as follows:

$$\varepsilon_{r,1} = \left(\frac{1-A_0}{1+A_0} \right)^2 \tag{3.24}$$

Similarly, the dielectric constant of the second layer is given as:

$$\varepsilon_{r,2} = \varepsilon_{r,1} \left(\frac{(1-A_0^2) e^{-\eta_0 \frac{\sigma_i t_i c}{2\varepsilon_{r,i}}} - A_1}{(1-A_0^2) e^{-\eta_0 \frac{\sigma_i t_i c}{2\varepsilon_{r,i}}} + A_1} \right)^2 \tag{3.25}$$

In general, the dielectric constant $\varepsilon_{r,n}$ of the nth layer can be expressed by the following equation:

$$\varepsilon_{r,n} = \varepsilon_{r,n-1} \left(\frac{(1-A_0^2) e^{-\frac{\eta_0 c}{2} \sum_{i=1}^{n-1} \frac{\sigma_i d_i}{\varepsilon_{r,i}}} - \sum_{i=1}^{n-2} \gamma_i A_i - A_{n-1}}{(1-A_0^2) e^{-\frac{\eta_0 c}{2} \sum_{i=1}^{n-1} \frac{\sigma_i d_i}{\varepsilon_{r,i}}} - \sum_{i=1}^{n-2} \gamma_i A_i + A_{n-1}} \right)^2 , for\, n = 2, ..., N \tag{3.26}$$

3.4.4 Estimation of Static Conductivity from Reflection Amplitudes

Following the plane wave model described in section 3.2, we will estimate the static conductivity. The PEC allows all the incident waves to be reflected completely; hence $r12 = 1$. This incorporation of PEC gives us the expression of attenuation as follows

$$\alpha = \frac{-1}{2d} \ln \left(\frac{A_2 \varepsilon_1 - 1}{4A_1 \sqrt{\varepsilon_1}} \right) \tag{3.27}$$

If we consider the pulse to be non-dispersive and incorporate the propagation constant considering high frequency and size of the scatterers to be less than the pulse wavelength, then attenuation can be simplified as follows:

$$\alpha = \frac{\sigma}{2\sqrt{\varepsilon_1}} \eta_0 \tag{3.28}$$

Here, $0 = 377$ and 1 equal to the previously calculated relative dielectric permittivity. Using the above equation we develop the equation of conductivity for 1st layer as follows:

$$\sigma_1 = \frac{2\sqrt{\varepsilon_1}}{\eta_0} \left[\frac{-1}{2d} \ln \left(\frac{A_2 \varepsilon_1 - 1}{4A_1 \sqrt{\varepsilon_1}} \right) \right] \tag{3.29}$$

The conductivity σ_n of the nth layer can now be expressed as follows:

$$\sigma_n = \frac{\sqrt{\varepsilon_{r,n}}}{d_n} \left(\frac{1}{\eta_0} \log \left[\frac{(1 - A_0^2)(\sqrt{\varepsilon_{r,n+1}} - \sqrt{\varepsilon_{r,n}})}{\sqrt{\varepsilon_{r,n+1}} \left(\sum_{i=1}^{n-1} \gamma_i A_i - A_n \right) - \sqrt{\varepsilon_{r,n}} \left(\sum_{i=1}^{n-1} \gamma_i A_i + A_n \right)} \right] - \sum_{i=1}^{n-1} \frac{\sigma_i d_i}{\sqrt{\varepsilon_{r,i}}} \right) \tag{3.30}$$

3.5 Summary

Now-a-days one of the frequent uses of GPR is finding out the layered media properties. In order to approximate the true values of electric permittivity, conductivity and thickness of different layers of underground medium, different parameters are to be considered. This makes the job very difficult to implement. With the advent of many optimization schemes, inversion methodsare able to closely approximate the true values of the media properties. But this process consumes much of the valuable time, which restricts the full potential of SFCW GPR. So in order to counteract this drawback, we usually apply layer stripping approach. This process is faster and able to approximate results much closer to inversion outputs. In order to obtain more accurate results, we perform layer stripping on the target layered media and feed the output for full wave modelling, which results in faster convergence to the true value.

Chapter 4

Results and Discussion

4.1 Experimental Model with a Single Layered Sand

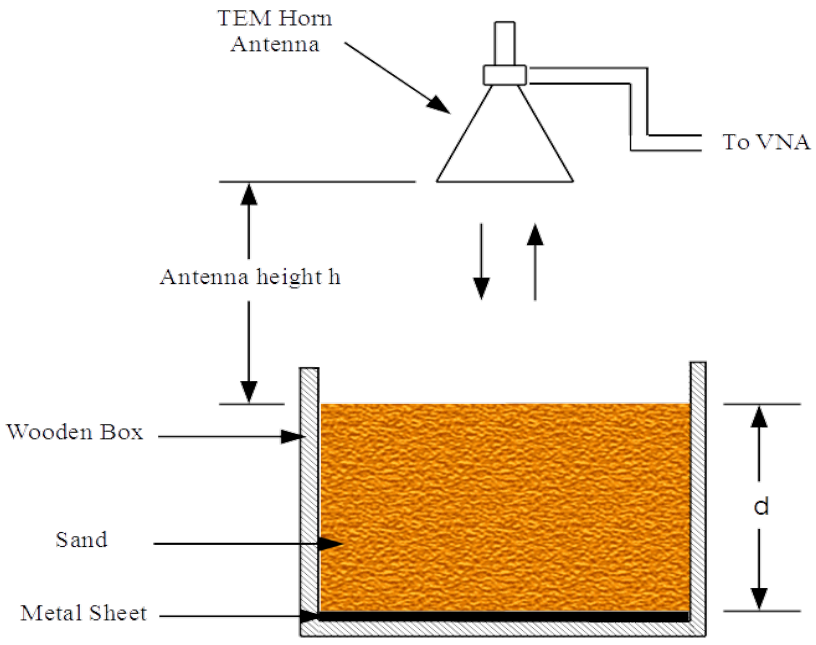

Figure 4.1: SFCW- Monostatic GPR Laboratory Experimental Setup

Description of System: The radar measurements were conducted on top of a wooden tank (138.598.5 cm) and a steel plate (12281 cm) at the bottom of the tank. The dimension of the antenna (BBHA 9120A, Schwarz beck Mess-Elektronik) is 24.52214.2 cm. The operating frequency band of the antenna is from 800 MHz

to 5 GHz. But the frequency range of 1000 MHz to 2000 MHz is used with a frequency step of 8 MHz to process the highest quality data. The metal plate is used to control the boundary condition for the radar measurement as well as to calibrate the radar system. Due to manual adjust-ment of the antenna stand, our height measurement inaccuracy was around 1 cm.

Calibration Process: Whenever air-coupled configuration is carried out, a static metal plate reflection should be carried out. In order to collect the free space pulse, the antenna is pointed sideways or upwards and a signal with no reflections is collected. Then a height calibrated file is created to correct the reflection amplitudes as a function of antenna's height above the ground surface.

Green Function: GPR wave propagation is given by Maxwells equations. Green function (i.e., the solution of the three-dimensional Maxwells equations) for EM waves travelling in multilayered media is well-known, and its known as the scattered x-directed electric field $Ex(\omega)$ at the field point for a unity-strength x-directed electric source $Jx(\omega)$ at the source point. An iterative approach to find the global reflection coefficients of the multilayered medium in the frequency domain can be used to find out Green function. Now in order to find the antenna characteristic coefficients, a system of equations similar to Eq. (3.13) with different known Green functions must be solved. Such functions belong to different configurations where measurements with the antenna are performed at different heights over a PEC.

Results of GPR detection with Full Wave Inversion:

1. Frequency Range Used: 1 GHz to 2 GHz
2. Relative Permittivity: 6.2
3. Conductivity at center frequency of 1.5 GHz: 33 mS/m
4. Linear variation in conductivity from 1 GHz to 2 GHz: 40 mS/m

Here we have applied each model order estimator on the modelled and measured data for a range of Time delay Bandwidth Product (TBP) from 0.6 to 0.9.

We have received different relative permittivity, conductivity and thickness values for each subband for each TBP. Then we have put a bound of 5% on the values obtained by full wave modelling. So the percentage of subbands who are within the bound are plotted for both cases of R-MUSIC and TLS-ESPRIT, for each TBP.

4.2 Results

Layer Stripping with Super-Resolution Algorithms: In order to estimate the layer properties, we have adopted two main super-resolution algorithms of R-MUSIC and TLS-ESPRIT. In order to ob-tain correct time delay and amplitude estimates, correct model order estimates have been obtained by MDL and EIF methods.

We have obtained our findings for both Modelled as well as Measured GPR data.

Synthetically Modelled Layered Media: Here we have provided the values of permittivity, conduc-tivity and thickness of the layered media and extracted the Greens function for modelled data. In order to obtain results for different TBP, we have to change the thickness of the layered media by keeping frequency of operation constant.

Practically Measured Layered Media: Upon obtaining the S11 parameters of the layered media from the VNA, they are fed into the radar-antenna model to extract Greens function for measured data. In order to obtain results for different TBP, we have to change the frequency of operation keeping the thickness of the layered media unchanged.

We have used a 5% bound from the actual parameter values for Bounded Percentage of Correct Estimation (BPCE).

For both synthetic and measured data, we will conclude the following points using suitable simulations:

1. **Estimation of better Effective Bandwidth for proper parameter estimation**

Synthetic Case: Upon comparing the estimates obtained from full wave modelling and comparing them to all the subbands of each TBP, we get the following distribution of Effective Bandwidth percentage for the nearest estimation to FWM data for each TBP, considering both R-MUSIC and TLS-ESPRIT:

For EIF order estimator:

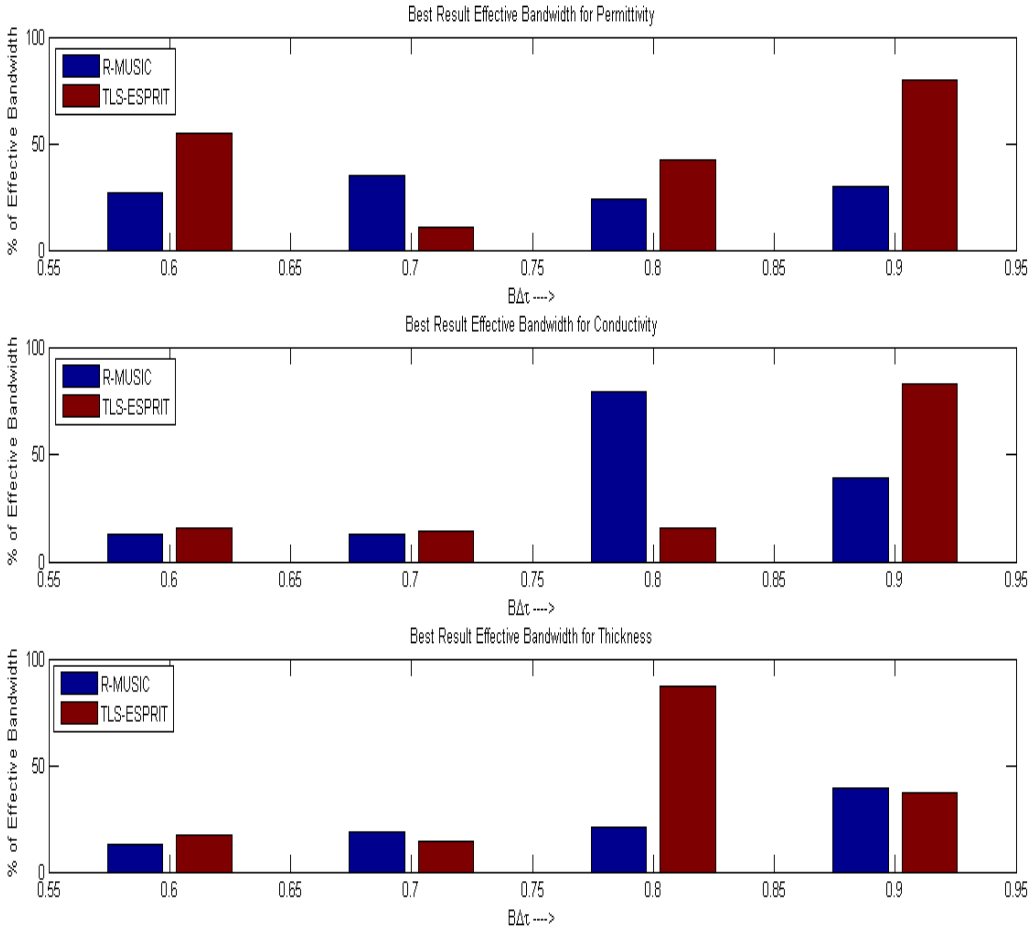

Figure 4.2: Best case Effective Bandwidth using EIF order estimator with modelled data

For MDL order estimator:

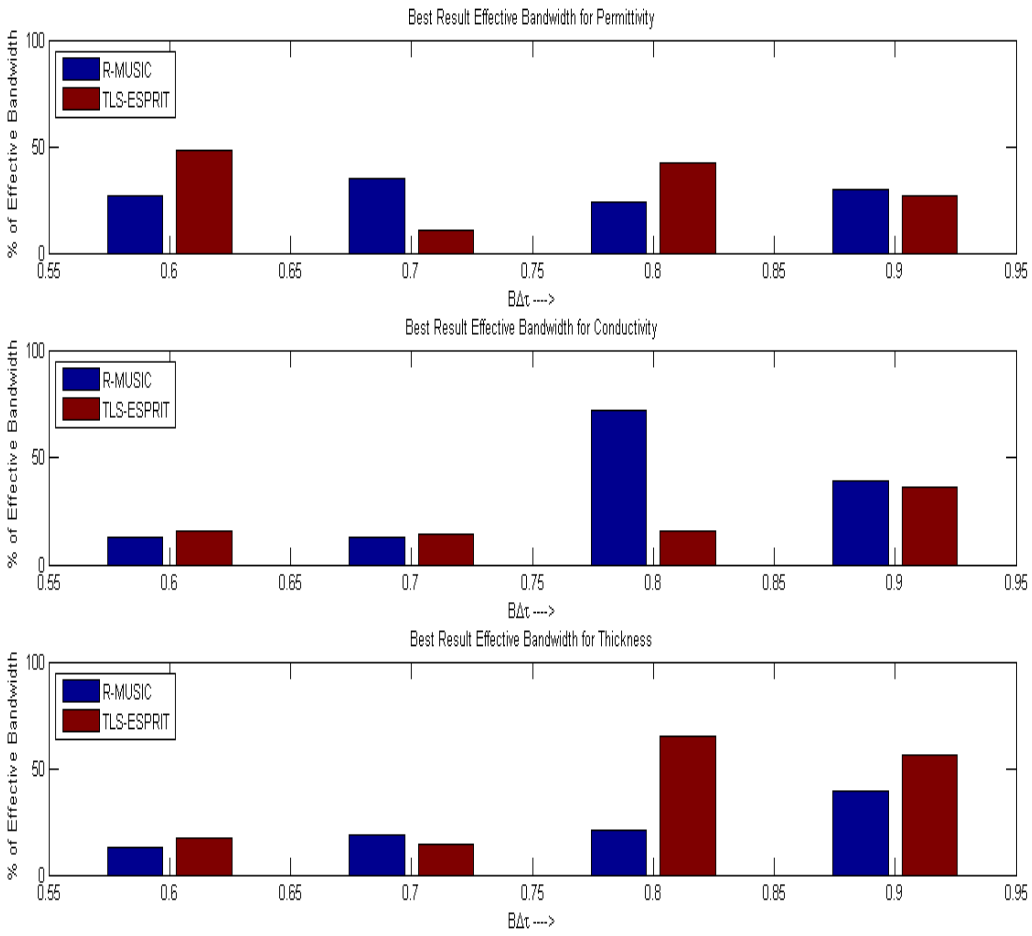

Figure 4.3: Best case Effective Bandwidth using MDL order estimator with modelled data

Comparing the percentages of Effective Bandwidth for TBP from 0.6 to 0.9 considering both R-MUSIC and TLS-ESPRIT, and obtaining percentage of times the percentage of Effective Bandwidth was under 50%, we get the following results:

(Results shows % of Effective Bandwidth greater than 50)

For EIF:

R-MUSIC: 91.6667 %

TLS-ESPRIT: 83.3333 %

For MDL:

R-MUSIC: 91.6667%

TLS-ESPRIT: 66.6667%

Measured Case: Upon comparing the estimates obtained from full wave modelling and comparing them to all the subbands of each TBP, we get the following distribution of Effective Bandwidth percentage for the nearest estimation to FWM data for each TBP, considering both R-MUSIC and TLS-ESPRIT:

For EIF order estimator:

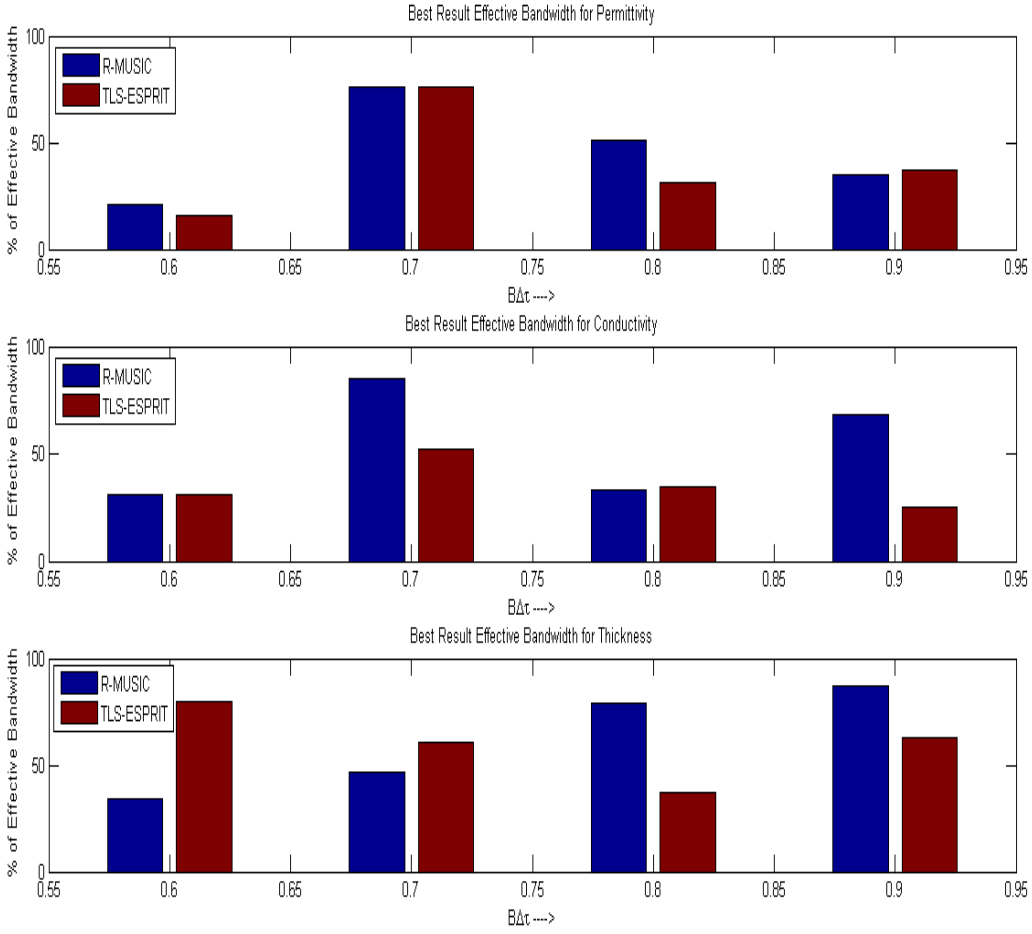

Figure 4.4: Best case Effective Bandwidth using EIF order estimator with measured data

For MDL order estimator:

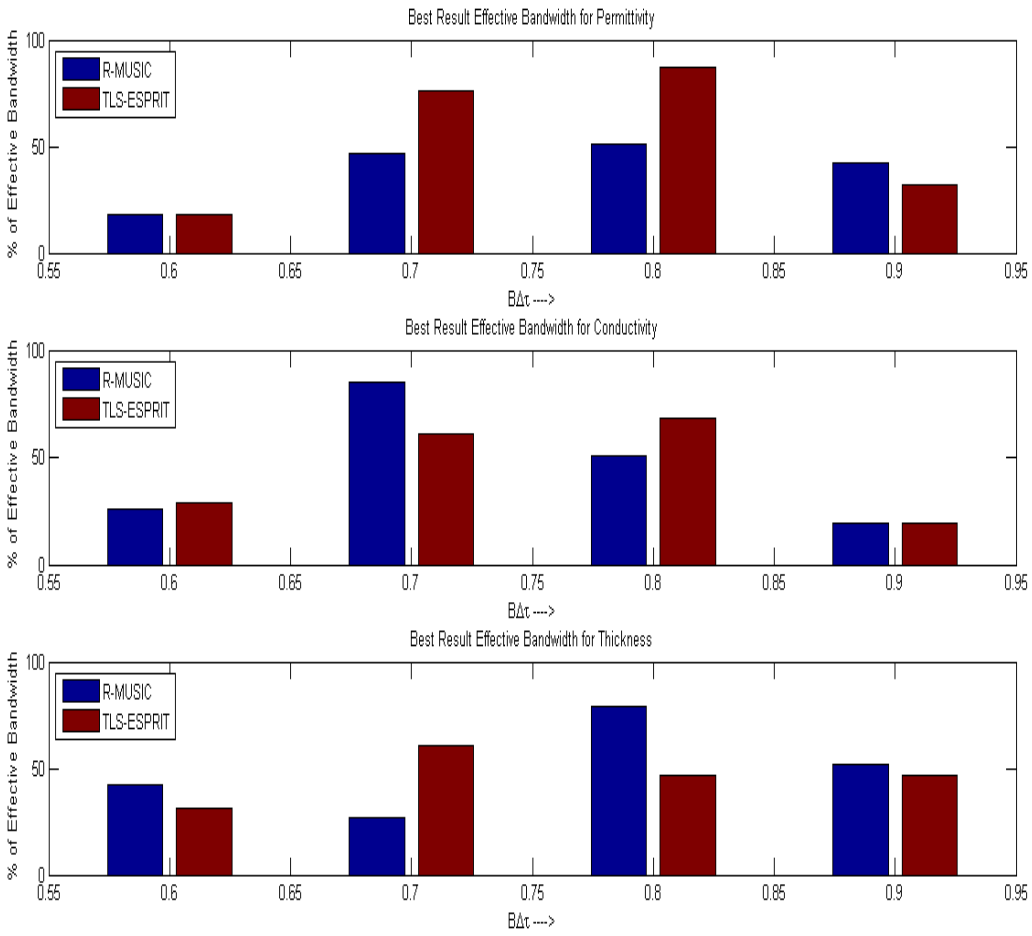

Figure 4.5: Best case Effective Bandwidth using MDL order estimator with measured data

Comparing the percentages of Effective Bandwidth for TBP from 0.6 to 0.9 considering both R-MUSIC and TLS-ESPRIT, and obtaining percentage of times the Effective Bandwidth was under 50% of the entire bandwidth, we get the following results:

(Results shows % of Effective Bandwidth greater than 50)

For EIF:

R-MUSIC: 50 %

TLS-ESPRIT: 58.3333 %

For MDL:

R-MUSIC: 58.3333%

TLS-ESPRIT: 58.3333%

We can therefore conclude that for TBP less than 1, we can get best parameter estimates if the percentage of Effective Bandwidth is less than 50. This corresponds with the fact that the decorrelation performance of the spatial smoothing techniques increases for percentage of Effective Bandwidth less than 50 [20]. And hence for TBP less than 1, the correlated data are decorrelated and we get good estimates of the parameters for percentage of Effective Bandwidth less than 50.

For TBP greater than 1, we can get best parameters for percentage of Effective Bandwidth both greater and lower than 50. In order to prove the above statement, we have observed GPR received signal with TBP of 1.5 and 2 for measured data. We get the following results:

Case I: TBP = 1.5 (Results shows % of Effective Bandwidth less than 50)

For EIF:

R-MUSIC: 100 %

TLS-ESPRIT: 33.3333 %

For MDL:

R-MUSIC: 66.6667%

TLS-ESPRIT: 66.6667%

Case II: TBP = 2 (Results shows % of Effective Bandwidth greater than 50)

For EIF:

R-MUSIC: 100 %

TLS-ESPRIT: 100 %

For MDL:

R-MUSIC: 33.3333%

TLS-ESPRIT: 100%

2. **Estimation of better Source Number Estimator for proper parameter estimation**

   In order to estimate the better order estimator between MDL and EIF, let us observe the following two plots:

   For EIF order estimator:

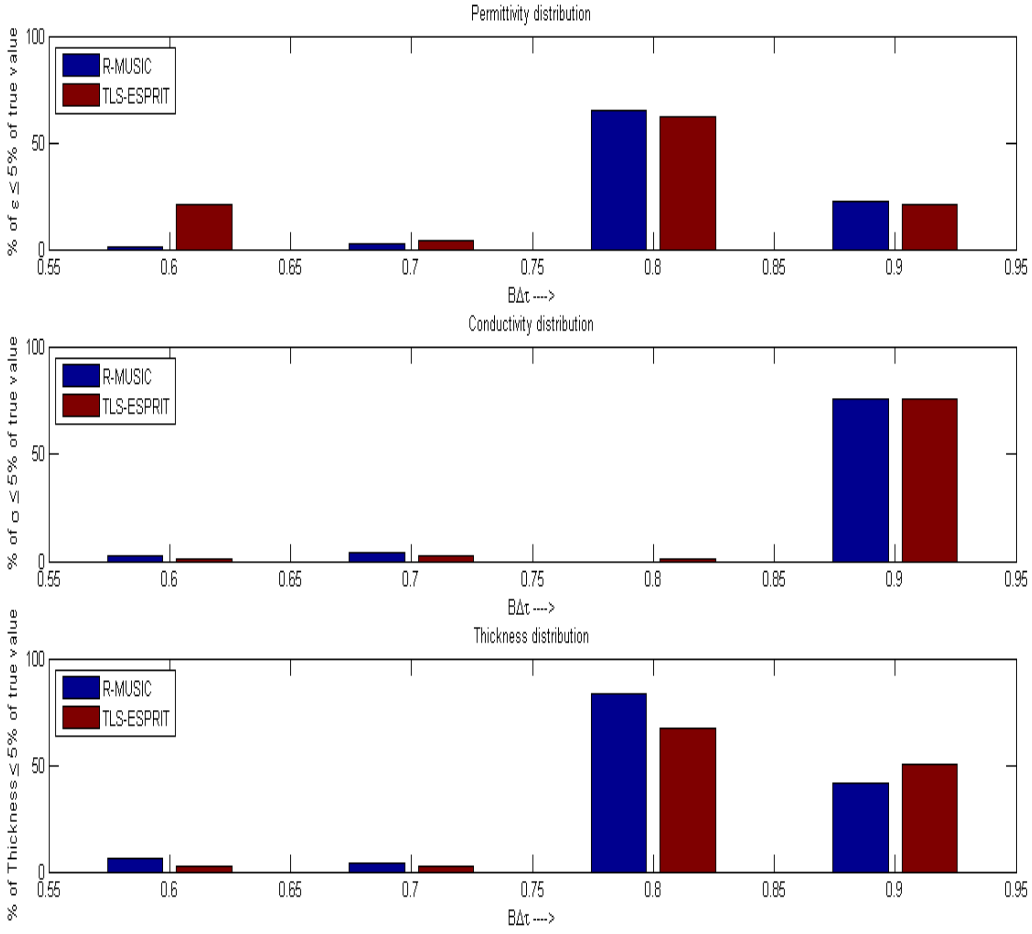

Figure 4.6: BPCE for EIF order estimator

For MDL order estimator:

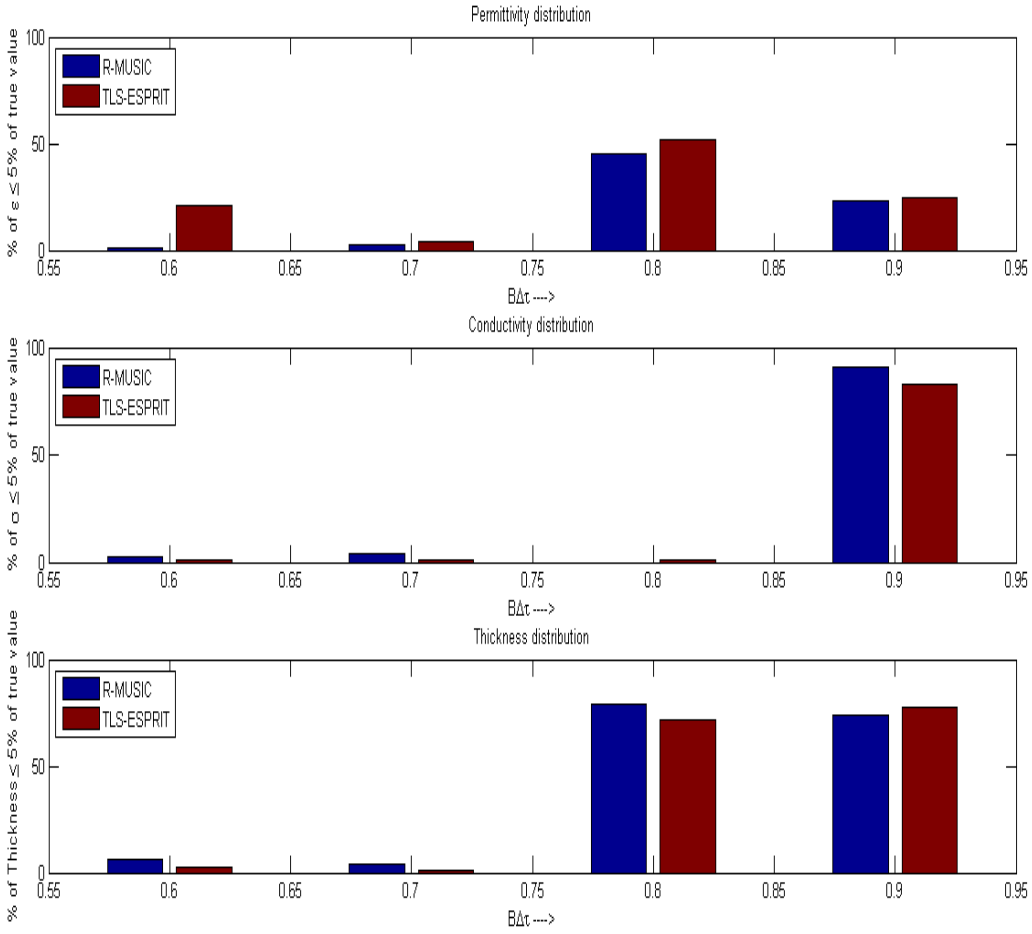

Figure 4.7: BPCE for MDL order estimator

Upon comparing permittivity, conductivity and thickness, with BPCE for TBP from 0.6 to 0.9, we observe that EIF gives more correct estimates of the parameters compared to MDL. Hence, **EIF** can be considered as the better signal source estimator than MDL. This outcome can be confirmed with [9]. Upon getting the better order estimator, we will focus our results on the outputs obtained from EIF estimator only.

3. **Estimation of better Subspace Model Estimator for proper parameter estimation**

We have observed the closest estimations of layered media parameters in comparison to full wave modelling. We will present the best estimations for each TBP and for both R-MUSIC and TLS-ESPRIT.

Synthetic Case:

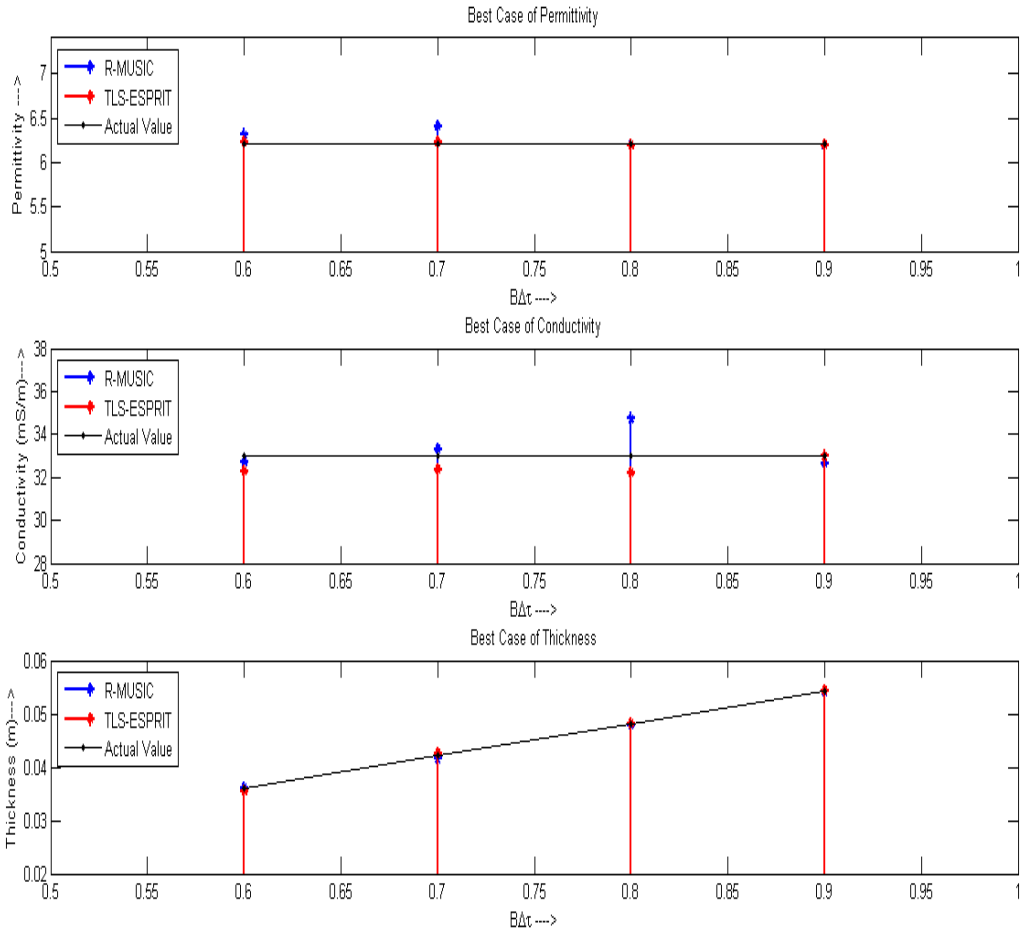

Figure 4.8: Best Case parameters estimation for different TBPs from modelled data

Measured Case:

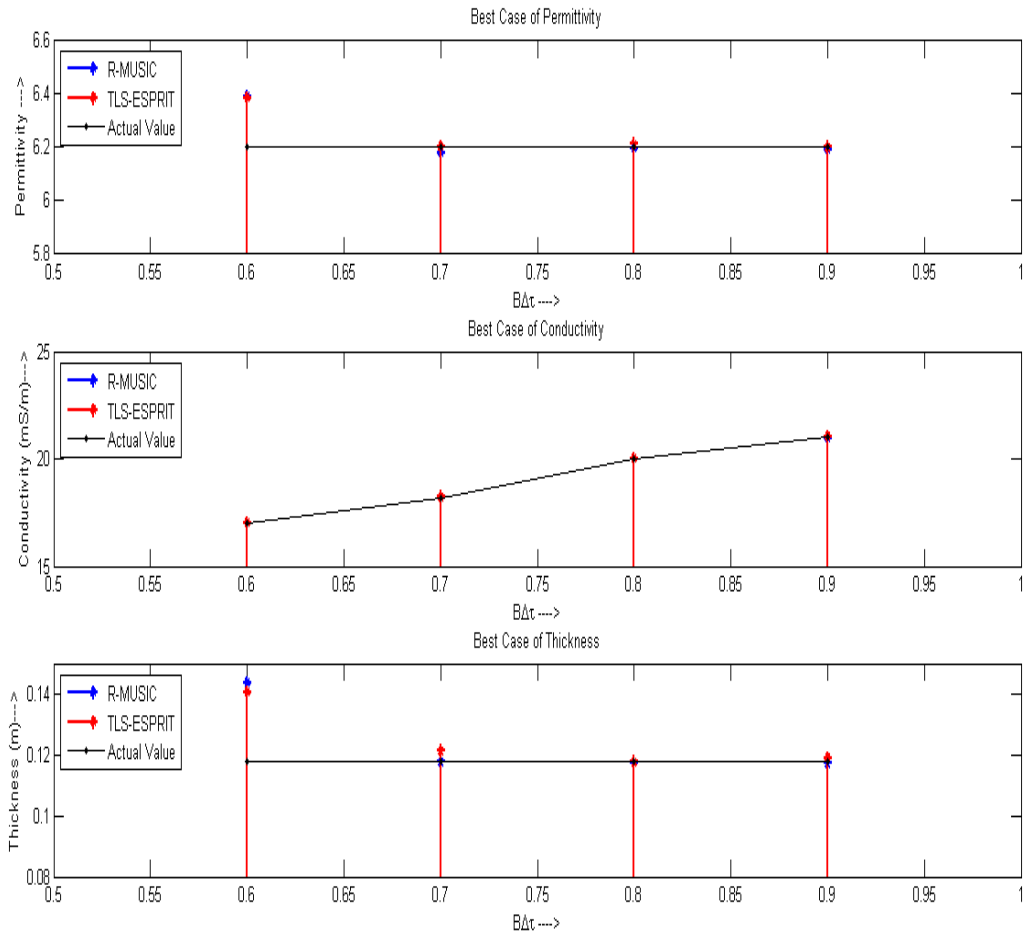

Figure 4.9: Best Case parameters estimation for different TBPs from measured data

Upon analyzing the values of each of the parameters for all TBPs, and finding the error percentage w.r.t. to full wave modelled output, we get that **TLS-ESPRIT** gives the overall minimum error considering TBP from 0.6 to 0.9.

4. **Comparison of Layered Media Parameters**

Measured Data: Here we have compared the layered media parameters for each TBP with EIF order estimator.

Table 4.1: Comparison of Layered Media Parameters for Measured Data

TBP –>		0.6	0.7	0.8	0.9
Bandwidth of Operation (MHz)		306	357	408	460
Center Frequency (MHz)		1153	1178	1204	1230
Permittivity	FWM	6.2	6.2	6.2	6.2
	R-MUSIC	6.3912	6.1802	6.1994	6.1913
	TLS-ESPRIT	6.3880	6.2026	6.2124	6.2010
Conductivity (mS/m)	FWM	17	18.2	20	21
	R-MUSIC	17.01	18.2270	20.0079	20.9713
	TLS-ESPRIT	17.0436	18.2270	20.0002	21.0228
Thickness (cm)	FWM	11.8	11.8	11.8	11.8
	R-MUSIC	14.37	11.77	11.75	11.71
	TLS-ESPRIT	14.06	12.12	11.77	11.91

Synthetic Data: Here we have compared the layered media parameters for each TBP with EIF order estimator.

Table 4.2: Comparison of Layered Media Parameters for Synthetic Data

TBP –>		0.6	0.7	0.8	0.9
Bandwidth of Operation (MHz)		1000	1000	1000	1000
Center Frequency (MHz)		1500	1500	1500	1500
Permittivity	FWM	6.2	6.2	6.2	6.2
	R-MUSIC	6.3104	6.4005	6.1998	6.1891
	TLS-ESPRIT	6.2272	6.2241	6.1894	6.1993
Conductivity (mS/m)	FWM	33	33	33	33
	R-MUSIC	32.7004	33.3059	34.7307	32.6620
	TLS-ESPRIT	32.2872	32.3579	32.2033	32.9698
Thickness (cm)	FWM	3.6145	4.2169	4.8193	5.4217
	R-MUSIC	3.61	4.15	4.79	5.42
	TLS-ESPRIT	3.54	4.26	4.82	5.43

4.3 Discussion

We have worked with a single layered wet soil media with a PEC at the base. Assuming that the correct estimates of the target parameters are known to us by using full wave modelling, we have shown how different methods are used to correctly estimate the target parameters.

To analyze the best Effective Bandwidth range, we have compared the actual value (obtained from full wave modelling) with each value obtained from different Effective Bandwidths and found the least error for both TLS-ESPRIT and R-MUSIC and similarly for all TBP.

To analyze the best signal source number estimator, we have compared the actual value with each value obtained from different Effective Bandwidths. Then we have selected the percentage of those values which are within 5% of the actual value. And this is repeated for every TBP. So, greater the BPCE, better is the order estimation of the estimator.

To analyze the better of the two subspace model estimators, we compared the values obtained by both TLS-ESPRIT and R-MUSIC for the specified Effective Bandwidth for each TBP with the actual value. Then we find the error percentage for each parameter to be estimated and for each TBP. We concluded best estimator for each parameter to be estimated and for each TBP. Then by observation we could find out the better estimator of the two.

Chapter 5

Conclusions and Future Work

5.1 Conclusion

Full Wave Modelling gives us very accurate estimation of subsurface layered media parameters. But due to its impractical nature to real life GPR measurements, an alternative approach was put to use. The method of layer stripping was implemented on one layered soil media. Layer stripping method is very fast and can be used in mobile GPR operations. The estimates of the parameters via layer stripping approach is well within 5% of the value estimated by full wave modelling. As a result, if the estimates of layer stripping are used as input to full wave model, then it would take very less time to converge to the best estimate. This will save much computational time for full wave modelling.

We were able to conclude the following points:

1. **Empirical Indicator Function (EIF) performs better than Minimum Description Length (MDL)** in estimating the correct number of correlated GPR signal sources.

2. Spatial smoothing is done in order to decorrelate the correlated GPR received signals. In order to do that the entire bandwidth is sub divided into sub bands of equal lengths. Then smoothing techniques are applied on those sub bands.

The length of the final smoothed sub band is called Effective Bandwidth. Now we may get different estimates of parameters for different Effective Bandwidths. It is known that Effective Bandwidth less than 50% of the entire bandwidth results in increase in decorrelation performance.

Considering the fact that we have used correlated data, we are getting best estimates of different parameters with percentage of Effective Bandwidth less than 50.

Now if uncorrelated data is used, then the proper parameter values can occur in any band of Effective Bandwidth. This is proved by taking a data with TBP of 1.5 which gives good estimates below 50% of Effective Bandwidth and a data with TBP of 2 which gives good estimates above 50% of Effective Bandwidth.

Hence, we can conclude that it is advisable to **obtain the estimates of parameters for percentage of Effective Bandwidth less than 50**.

3. For the range of TBP from 0.6 to 0.9, we **obtained better estimates using TLS-ESPRIT in comparison to R-MUSIC**.

5.2 Future Work

1. Find and use other model order estimators which will give higher performance than both MDL and EIF.
2. Implement Compressive Sensing approach to represent super resolution properties owing to the sparsity property of the GPR target media.
3. Perform the experiment using water media and two layered soil media.
4. Introduce antenna height error along with thermal noise and observe the changes in the output for both the cases.
5. Try to obtain more accurate range of Effective Bandwidth for best estimation of target parameters.

Bibliography

[1] A. Benedetto and L. Pajewski, "Civil engineering applications of ground penetrating radar," *Springer Transactions in Civil and Environmental Engineering*, 2015.

[2] J. Leckebusch, "Ground-penetrating radar: a modern three-dimensional prospection method," *Archaeological prospection*, vol. 10, no. 4, pp. 213–240, 2003.

[3] J. D. Irving, *Estimation and correction of wavelet dispersion in ground penetrating radar data*. PhD thesis, University of British Columbia, 2000.

[4] S. Lambot *et al.*, *Hydrogeophysical characterization of soil using ground penetrating radar*. PhD thesis, Ph. D. thesis, Catholic Univ. of Louvain, Louvain-la-Neuve, Belgium, 2003.

[5] A. N. Duc and B. H. Phu, "A detail design and evaluation of stepped frequency continuous wave ground penetrating radar systems," *International Journal of Research in Wireless Systems*, vol. 3, no. 1, 2014.

[6] Q. Cheng and H. Yingbo, "A review of parametric high-resolution methods," *High-resolution and robust signal processing (H. Yingbo, A. Gershman, and Q. Cheng, eds.), Marcel Dekker*, 2003.

[7] P. Stoica and R. L. Moses, *Spectral analysis of signals*. Pearson/Prentice Hall Upper Saddle River, NJ, 2005.

[8] P.-J. Chung, "Parameter estimation: Subspace methods,"

[9] C.-I. Chang and Q. Du, "Estimation of number of spectrally distinct signal sources in hyperspectral imagery," *Geoscience and Remote Sensing, IEEE Transactions on*, vol. 42, no. 3, pp. 608–619, 2004.

[10] H. Zhonglai and Z. Jianzhong, "Multi-parameter spectral inversion for gpr signals of subsurface layered media," in *Ground Penetrating Radar (GPR), 2012 14th International Conference on*, pp. 274–280, IEEE, 2012.

[11] S. Lambot, E. Slob, I. van den Bosch, B. Stockbroeckx, B. Scheers, and M. Vanclooster, "Estimating soil electric properties from monostatic ground-penetrating radar signal inversion in the frequency domain," *Water Resources Research*, vol. 40, no. 4, 2004.

[12] A. Kalogeropoulos, J. Van Der Kruk, J. Hugenschmidt, J. Bikowski, and E. Brühwiler, "Full-waveform gpr inversion to assess chloride gradients in concrete," *Ndt & E International*, vol. 57, pp. 74–84, 2013.

[13] S. Maiti, S. K. Patra, and A. Bhattacharya, "Modelling gpr for characterization of subsurface em properties," in *Microwave and RF Conference, 2013 IEEE MTT-S International*, pp. 1–4, IEEE, 2013.

[14] S. Lambot, L. Weihermüller, J. A. Huisman, H. Vereecken, M. Vanclooster, and E. C. Slob, "Analysis of air-launched ground-penetrating radar techniques to measure the soil surface water content," *Water Resources Research*, vol. 42, no. 11, 2006.

[15] S. Lahouar, *Development of data analysis algorithms for interpretation of ground penetrating radar data*. PhD thesis, Virginia Polytechnic Institute and State University, 2003.

[16] D. J. Daniels, *Ground penetrating radar*. Wiley Online Library, 2005.

[17] A. Loulizi, I. L. Al-Qadi, and S. Lahouar, "Optimization of ground-penetrating radar data to predict layer thicknesses in flexible pavements," *Journal of transportation engineering*, vol. 129, no. 1, pp. 93–99, 2003.

[18] M. Gonzalez Huici, *Accurate ground penetrating radar numerical modeling for automatic detection and recognition of antipersonnel landmines*. PhD thesis, Universitäts-und Landesbibliothek Bonn, 2013.

[19] C. Le Bastard, V. Baltazart, Y. Wang, and J. Saillard, "Thin-pavement thickness estimation using gpr with high-resolution and superresolution methods," *Geoscience and Remote Sensing, IEEE Transactions on*, vol. 45, no. 8, pp. 2511–2519, 2007.

[20] S. M. Shrestha and I. Arai, "Signal processing of ground penetrating radar using spectral estimation techniques to estimate the position of buried targets," *EURASIP Journal on Advances in Signal Processing*, vol. 2003, no. 12, pp. 1198–1209, 1900.

[21] "Line spacing in latex documents." `http://www.malags.com/getattachment/Innovation/GPR-Explained/MALA-GPR-principle.jpg/`. Accessed June 1, 2015.